NACA RM No. A8F22

UNCLASSIFIED Copy No. 5

[redacted]

RM No. A8F22

6 OCT 1948

RESEARCH MEMORANDUM

INVESTIGATION AT SUPERSONIC SPEED (M=1.53) OF THE PRESSURE DISTRIBUTION OVER A 63° SWEPT AIRFOIL OF BICONVEX SECTION AT SEVERAL ANGLES OF ATTACK

By John W. Boyd, Elliott D. Katzen,
and Charles W. Frick

Ames Aeronautical Laboratory,
Moffett Field, Calif.

CLASSIFICATION CANCELLED

Authority NACA R 72389 Date 8/18/54

m.H.A. 8/31/54 See

CLASSIFIED DOCUMENT

This document contains classified information affecting the National Defense of the United States within the meaning of the Espionage Act, USC 50:31 and 32. Its transmission or the revelation of its contents in any manner to an unauthorized person is prohibited by law. Information so classified may be imparted only to persons in the military and naval services of the United States, appropriate civilian officers and employees of the Federal Government who have a legitimate interest therein, and to United States citizens of known loyalty and discretion who of necessity must be informed thereof.

NATIONAL ADVISORY COMMITTEE
FOR AERONAUTICS

WASHINGTON
September 24, 1948

UNCLASSIFIED

N A C A LIBRARY
LANGLEY MEMORIAL AERONAUTICAL
LABORATORY
Langley Field, Va.

[redacted]

NASA Technical Library
3 1176 01434 4601

UNCLASSIFIED

NATIONAL ADVISORY COMMITTEE FOR AERONAUTICS

RESEARCH MEMORANDUM

INVESTIGATION AT SUPERSONIC SPEED (M=1.53) OF THE PRESSURE DISTRIBUTION OVER A 63° SWEPT AIRFOIL OF BICONVEX SECTION AT SEVERAL ANGLES OF ATTACK

By John W. Boyd, Elliott D. Katzen,
and Charles W. Frick

SUMMARY

The results of an investigation at supersonic speed of the distribution of pressure over the surface of a swept airfoil of biconvex section at various angles of attack are presented. The airfoil used for the experiment was composed of sections 7 percent thick in streamwise planes and was swept back 63° 45'. The plan form of the wing was such as to give an aspect ratio of 1.66 and a taper ratio of 1. Tests were made at a Mach number of 1.53 over a Reynolds number range of 0.48×10^6 to 3.0×10^6 at angles of attack up to 10°.

The measurements have been compared with supersonic lifting-surface theory. Good agreement between theory and experiment is found except over the regions of the airfoil surface influenced by the subsonic trailing edge and the tips. Within these regions, theory and experiment disagree. The disagreement is not consistent at all angles of attack. Analysis of the data shows that the flow is separated near the trailing edge and, hence, the effect of viscosity is predominant. The degree of separation on the upper and lower surfaces varied with angle of attack with a consequent variation in the chordwise distribution of the additional lift.

Comparison of the measured chordwise distribution of lift with the results of tests of airfoil sections at transonic speeds indicates that the separation effects may be attributed to shock-wave boundary-layer interaction. This phenomenon may be unusually severe for this airfoil because of its thickness distribution.

Although the normal-force and pitching-moment coefficients determined from a mechanical integration of the experimental pressures are in good agreement with theory at the low angles of attack, the agreement must be viewed as being largely fortuitous

[redacted]

UNCLASSIFIED

because of the discrepancy between theoretically and experimentally determined pressures.

INTRODUCTION

Theoretical solutions for the distribution of pressure at supersonic speeds over the surface of lifting wings are, in general, possible only if the nonlinear equations of motion are approximated by linear equations and viscosity effects are disregarded. The approximations thereby introduced, of course, limit the applicability of the solutions to cases where the viscosity effects and the nonlinear terms are not significant.

The range of Mach numbers, airfoil thicknesses, angles of attack, and Reynolds numbers for which the theory should give reasonable accuracy can be estimated to some extent from mathematical considerations and from a general knowledge of viscous effects. It is desirable, however, to determine the magnitude of the error involved in using the theory to treat cases where it does not strictly apply but for which at least an approximate solution is required by the designer. This must be done, for the present at least, by a series of careful experiments.

The present report is the second of two publications presenting results of an experiment at one supersonic Mach number (M=1.53). The first report (reference 1) discussed the distribution of pressure over the swept airfoil at zero lift. The present report is intended to serve as a partial check of the validity of supersonic lifting-surface theory for swept wings.

The method of reference 2, which treats airfoils with subsonic trailing edges, was used to compute the theoretical lifting pressure distribution. References 3 and 4 might have been used, at least for portions of the airfoil surface ahead of the Mach line from the root trailing edge.

SYMBOLS

Re	Reynolds number based on the streamwise chord of 6 inches
α	angle of attack of the airfoil
C_N	normal-force coefficient

$C_{m_{c/2}}$	pitching-moment coefficient about centroid of area based on 6-inch chord
$\frac{p_u - p_l}{q_o \alpha}$	lifting-pressure coefficient per degree angle of attack
p_u	local static pressure on the upper surface of the airfoil
p_l	local static pressure on lower surface of the airfoil
q_o	free-stream dynamic pressure
p_o	free-stream static pressure
$\frac{p_o - p_w}{q_o}$	stream static pressure coefficient
p_w	reference static pressure
x/c	percent of chord
x	streamwise position from leading edge of airfoil
c	wing chord

DESCRIPTION OF APPARATUS

The experimental investigation was performed in the Ames 1- by 3-foot supersonic wind tunnel No. 1. This tunnel is of the closed-return variable-pressure type operated at present with a fixed nozzle designed for a Mach number of 1.53 in a 1- by $2\frac{1}{2}$-foot test section. A detailed description of the tunnel is given in reference 5.

Model and Model Support

The model selected for the investigation was composed of constant-chord, symmetrical biconvex sections in planes perpendicular to the leading edge which was swept back 63°45'.[1] Circular-arc sections were chosen for two reasons: First, because the theory used to predict the thickness pressure distribution is restricted to airfoils with sharp leading edges and, second, because the construction of the model was much simplified. The thickness of the sections in planes parallel to the stream was chosen as 7 percent primarily from a consideration of model strength.

---

[1] The airfoil sections in planes parallel to the stream consist of elliptical arcs.

Figures 1 and 2 show the airfoil mounted in the tunnel, and figure 3 gives all pertinent dimensions of the model.

A more detailed description of the model and the model support system is given in reference 1, which also discusses the precautions that were taken to minimize disturbances in the tunnel air stream that the model support system might have caused.

ANALYSIS OF DATA

Air-Stream Characteristics

In order to determine the character of the flow as influenced by the model support system, an investigation of the wind-tunnel air stream was made prior to actual tests of the airfoil. Static pressure surveys of the stream were made parallel to the axis of the tunnel at three positions across the stream in the horizontal plane in which the model was placed.

These surveys were made with a static-pressure probe consisting of a 100-caliber ogival needle, 0.10 of an inch in diameter. Pressure orifices were placed in the needle at a position for which an analysis using linear theory indicated that the local pressure was equal to that of the stream.

The results of the static-pressure survey are given in figure 4. The Reynolds numbers indicated in this figure are based on the 6-inch chord of the wing at tunnel total pressures of 3, 12, and 24 pounds per square inch, respectively. The data are given as the difference between the pressure measured with the needle and the pressure measured by the test-section reference static-pressure orifice in terms of the dynamic pressure of the stream. This reference pressure orifice is located on the side wall of the tunnel 3.06 inches ahead of the apex of the leading edge of the airfoil. The pressure coefficients are plotted as a function of the distance downstream from the location of this orifice. The location of the wing is shown in each figure.

Examination of these data and comparison with previous surveys of the stream along the center line of the tunnel without the model support system show that practically the only effect of the support system was the propagation of a weak compression wave in the stream which can be traced to the leading edge of the model support plate. This wave, which appears as a pressure discontinuity in figure 4(a) 4 inches downstream of the position of the test-section reference pressure orifice, becomes of negligible magnitude at a small distance outboard of the support plate (figs. 4(b) and (c)). Rotating the side plate through the range of angles of attack does not alter the magnitude of this compression wave.

This wave was originally believed to be due to the fact that the flat outer surface of the support plate was not parallel to the stream, but further tests with the inclination of the plate varied showed merely a change in the general pressure level without altering the strength of the wave. It seems probable that the disturbance results because it is impossible to produce a leading edge sharp enough in terms of molecular dimensions to prevent the formation of a detached shock wave even though the flat side of the plate is alined with the stream. The formation of a boundary layer on the plate also probably makes the edge of the plate effectively blunt.

The existence of this disturbance had very little effect on the stream static pressure distribution over the region in which the wing was placed. The pressure over this region was within $\pm1\frac{1}{2}$ percent of the average dynamic pressure of the stream.

REDUCTION OF DATA

The pressure data were recorded by photographing the manometer board. The data were then plotted directly in terms of pressure coefficient through the use of a film "reader." The static-pressure corrections were made after plotting. The corrections to the measured pressure data were made by subtracting from the reading for each orifice the difference in stream static-pressure coefficient between the value at the position of the orifice and the average value over the region of the wing. This method of correcting the pressure coefficients is such that the same static pressure correction is applied to both the upper and lower surface pressures. Since the lifting-pressure coefficients were obtained by taking the difference between the upper and lower surface pressures, there was effectively no static-pressure correction applied to the lifting-pressure coefficients. However, the true correction, which is very complex, may be, in local regions, twice as large as the correction applied, depending on whether or not the disturbance is reflected from the wing. The precision of the correction will be discussed later.

The normal-force and pitching-moment coefficients of the airfoil were obtained by a process of mechanical integration. The pressure distribution diagrams for each spanwise station were integrated for each angle of attack to obtain the section normal-force coefficient. The plots of section normal-force coefficient against percent semispan were integrated to obtain the total normal-force coefficient of the airfoil at each angle of attack. A comparison of the theoretical normal-force coefficients obtained from a mechanical integration of the theoretical pressure-distribution diagrams with the theoretical normal-force coefficients determined from an analytic integration reveal an error of about 8 percent in the mechanically integrated normal-force coefficients. The experimental normal-force coefficients obtained by mechanical integration are possibly also within ±8 percent of the true value.

PRECISION

Since the flow in the tunnel is free of strong shock waves, there remain only six major items which may cause inaccuracies in the determination of the experimental pressure distribution over the airfoil:

1. Errors of the pressure probe used to measure the static pressure in the stream
2. The error involved in using a superposition process to correct for the variation in the stream static pressure over the region of the wing
3. The error involved in reducing the data with a film reader
4. Errors of the individual wing pressure orifices
5. The error introduced by variations in stream angle
6. The error involved in setting the angle of attack

No means for determining the inaccuracy of the pressure probe is available at present. It is estimated, however, from calculation of the pressure distribution over the probe and from what is generally known about the inaccuracies of pressure orifices that the pressure probe measures the local-stream static pressure within $\pm \frac{1}{2}$ of 1 percent. This is the accuracy of the dynamic pressure used in obtaining pressure coefficients.

The correction made for the pressure variation in the stream, discussed previously, consists merely of a superposition process.

The same static pressure correction was applied to both the upper and lower surface pressures. However, if the disturbances, causing the static pressure variation in the stream, are finite shock waves, then the true correction is very complex, depending on whether or not the waves are reflected from the model. The correction may be twice as large on that surface of the airfoil from which the disturbance is reflected. However, a survey of the pressure distribution over a flat plate at zero angle of attack in the wind tunnel gave the same static pressure gradient as was indicated by the needle survey. Since any asymmetrical disturbances propagated from either the top or bottom of the tunnel would cause a different pressure gradient over the flat plate than that given by the needle, it appears that the major disturbances are either symmetrically disposed with respect to the top and bottom of the tunnel or that they originate from the side walls. In either case, the superposition process gives a very close approximation. Therefore, since the static-pressure variation over the region of the wing amounts to about $\pm 1\frac{1}{2}$ percent of the dynamic pressure, the accuracy of the correction would probably be within $\frac{1}{2}$ of 1 percent of the dynamic pressure if the superposition is 75 percent correct.

The use of the film reader in plotting pressure coefficients involves an error of about ±1/3 of 1 percent at the highest wind-tunnel pressures where most of the pressure measurements were made.

Examination of the data obtained from tests of the airfoil at zero lift shows that orifices at the same chordwise and spanwise positions on the upper and lower surfaces of the wing read the same pressure within $\frac{1}{2}$ of 1 percent of the stream dynamic pressure. This has been taken as the orifice error.

Surveys of the wind-tunnel stream show small stream angles existing over the region in which the wing was placed. It is evident from a study of the pressure data obtained for the airfoil at zero lift, however, that their influence was negligible since the lift due to the "induced camber" effect that should appear does not exist.

A measure of the final accuracy of the pressure distribution data can be obtained by taking the square root of the sum of the squares of the various probable inaccuracies. The final pressure coefficients are then found to approximate the true values within ±1 percent of the dynamic pressure.

The airfoil was set at an angle of attack with a propeller protractor which can be read accurately to within ±0.05 of a degree. Airfoil deflections under load were measured with a cathetometer and found to be negligible.

The absolute humidity was at all times kept below 0.0002 pound of water per pound of air so that the correction involved was negligible.

RESULTS AND DISCUSSION

Pressure Distribution

The experimental pressure coefficients, corrected for the static pressure variation in the stream, are given in table I for angles of attack from zero to 10° for two Reynolds numbers. These are the basic data from which the plotted data discussed later are derived. They are presented for use in any further analysis which the reader may wish to make.

Figure 5 shows a comparison between the theoretical and experimental chordwise distribution of lifting-pressure coefficient per degree angle of attack for the five spanwise stations of the airfoil for which the pressure distributions were measured. These data are for the highest test Reynolds number 3.0×10^6. It is evident that theory and experiment agree well except within the regions influenced by the subsonic trailing edge and the tip. (See fig. 3.) Examination of the data for pressure orifices near the trailing edge shows that the shape of the additional lift curve varies with angle of attack. A cross plot of the data for the orifice at 80 percent of the chord in figure 5(c), for example, shows a variation in the local lifting-pressure coefficient with angle of attack which is quite similar to the variation that occurs at subsonic speeds in the vicinity of the bevel of a beveled trailing-edge airfoil. For the angles of attack up to 4°, an increase in angle of attack results in negative lift. This "bevel effect" is well known to control-surface designers and has been proposed as a means of balancing control surfaces. (See reference 6.) This phenomenon depends on turbulent separation of the flow from both surfaces of the airfoil at zero lift. The reduction in the degree of separation on the lower surface that occurs when the angle of attack is increased provides the negative lift.

For the airfoil of the present investigation, the separation of flow near the trailing edge was noted from studies of the boundary-layer flow in reference 1, substantiating the conclusions reached from an examination of the pressure data presented herein. Since flow separation exists, no agreement between theory and experiment can be expected in this region of the airfoil.

It is interesting to note that some similarity exists between the results of figure 5 and the data of reference 7 which presents two-dimensional pressure-distribution characteristics for airfoil sections similar to those used for the wing of the present test. A comparison of the data indicates that the flow separation and its consequent effect on the lift distribution over the rear of the airfoil is due primarily to the chordwise-thickness distribution. The pressure data of reference 7 show that separation becomes more severe as the position of maximum thickness is moved rearward. Examination of unpublished schlieren photographs obtained during those same tests corroborate this conclusion.

A close correlation of the results of reference 7 with the data of the present test is not to be expected. Those results were obtained through tests of airfoil sections of 6-percent maximum thickness. As noted previously, the airfoil of the present test is 7 percent thick in streamwise planes and 15.9 percent thick in planes perpendicular to the leading edge. Which thickness is more significant is not clear, since the aspect ratio is so small that a perfect cylindrical or section-type flow does not exist.

The comparison suggests, however, that section data are in general useful in determining flow characteristics of swept airfoils even though cylindrical flow does not exist. It suggests further that the trailing-edge angle and chordwise-thickness distributions are important parameters at supersonic speeds and that care must be taken in selecting airfoil sections for swept wings.

The agreement between theoretical and experimental pressure distributions near the tip is poor, experiment showing a great deal more lift. This effect has been noted at subsonic speeds. The probability exists that there is lift added to the tip, because the vortex sheet discharged from the tip does not lie in the plane of the wing as theory assumes.[2] In addition, this effect may be due in part to the rapid thickening of the boundary layer in this region.

Figure 6 presents the chordwise variation of lifting-pressure coefficient per degree at five spanwise stations at 4° angle of attack for three test Reynolds numbers, 0.48×10^6, 1.85×10^6, and 3.0×10^6. The effect of the Reynolds number variation is negligible except within the region of influence of the subsonic trailing edge.

---

[2] The effect of the departure of the vortex sheet from the plane of the wing becomes of greatest importance for low aspect ratios and has been treated by Bollay in reference 8.

In this region a reduction in Reynolds number so influences the flow separation as to reduce the negative lift.

Although laminar separation was observed at the lowest Reynolds number at zero lift, this phenomenon disappeared as soon as the airfoil was given an appreciable angle of attack.

In reference 1 it was shown that through a calculation of the local Mach number on the surface of the airfoil by linear theory, it is possible to determine theoretically the curved line defining the foremost influence of the subsonic trailing edge. Good agreement between the pressure discontinuity so defined and the experimentally determined pressure discontinuity was shown at zero lift. (See reference 1.) For the airfoil at an angle of attack, however, examination of the pressure data of table I gives no clear evidence of a steep pressure increase as was noted at zero lift. This is probably due to the fact that on the upper surface of the airfoil the boundary layer thickens very rapidly as the angle of attack is increased because of the sharp leading edge. The existence of a sharp pressure rise or shock wave is, therefore, not discernible from the pressure data because the abrupt pressure rise is probably diffused by the thickened boundary layer as has been shown in reference 9. Studies of the boundary-layer flow, however, do indicate the existence of a curved pressure discontinuity. These studies are discussed later.

Boundary-Layer Studies

Use was made of the liquid-film technique, which has been discussed fully in reference 10, to investigate the character of the boundary flow. This method of visualizing the boundary-layer flow consists of applying a thin film of a slightly volatile liquid to the airfoil surface and observing the degree of evaporation from various portions of the airfoil to determine the relative areas of laminar and turbulent flow. The liquid-film streamers also give an indication of the direction of flow of the air in the boundary layer next to the airfoil surface.

Figure 7 shows flow studies at the highest test Reynolds number at 0°, 4°, and 8° angle of attack. The existence of turbulent separation at zero lift is indicated by the photograph of figure 7(a). The liquid-film streamers turn and flow along the airfoil-surface generators near the trailing edge. This confirms the existence of separation that was indicated by the pressure data.

At 4° angle of attack (fig. 7(b)), the separation is shown to be more extensive, extending forward to the pressure discontinuity propagated from the root trailing edge. This pressure discontinuity which probably is a shock wave, though the pressure data are not conclusive, is seen to be curved in a manner quite similar to that discussed in reference 1. As noted in reference 1, if the pressure discontinuity is bent back sufficiently so that it eventually lies along one of the airfoil generators, the airfoil has reached or exceeded its critical supersonic Mach number. This seems to be the case for the airfoil of the present test.

Examination of figure 7(b) shows a thin ridge of fluid lying just behind the leading edge. The existence of this ridge denotes a small region of laminar separation which is to be expected with a sharp leading edge.

At an 8° angle of attack (fig. 7(c)), the boundary layer has become so thick over the entire wing that it is impossible to place any interpretation on the liquid-film flow.

Normal Force and Pitching Moment

The normal-force and pitching-moment characteristics of the airfoil were determined by a mechanical integration of the lifting pressures over the area of the wing at the various test angles of attack. These data are plotted in figures 8 and 9 and are compared with the results calculated by the linear theory of reference 2. The results show good agreement between the theoretical normal-force-curve and moment-curve slopes through zero lift. This agreement is somewhat surprising, especially for the pitching moment, in view of the serious discrepancy between the theoretical and experimental pressure distributions near the trailing edge and tip, and hence may be viewed as being largely fortuitous.

CONCLUDING REMARKS

The results of the investigation show that theory and experiment are in good agreement in those regions of the airfoil not influenced by the subsonic trailing edge and the tip. Within the Mach cone of the root trailing edge, no correspondence between theory and experiment exists. The lack of agreement can be attributed to the occurrence of turbulent separation which renders the theory invalid in this region. Near the tip, the failure of the theory is believed to be due to boundary-layer effects and to the effects of the distortion of the discharged vortex sheet.

Comparison of the results of the experiment with section data at transonic Mach numbers, especially with regard to the separation of flow near the trailing edge, indicates that the thickness distribution of the airfoil is important.

The airfoil of the present test is apparently too thick to permit the use of the linear theory for an accurate estimation of the lifting pressures at the test Mach number. The thickness distribution also appears to be undesirable. Additional tests of airfoils composed of thinner sections with different thickness distributions are desirable, however, for the purpose of investigating the validity of the linear theory near a subsonic trailing edge.

Ames Aeronautical Laboratory,
National Advisory Committee for Aeronautics,
Moffett Field, Calif.

REFERENCES

1. Frick, Charles W., and Boyd, John W.: Investigation at Supersonic Speed ($M=1.53$) of the Pressure Distribution Over a 63° Swept Airfoil of Biconvex Section at Zero Lift. NACA RM No. A8C22, 1948.

2. Cohen, Doris: The Theoretical Lift of Flat Swept-Back Wings at Supersonic Speeds. NACA TN No. 1555, 1948.

3. Stewart, H.J.: The Lift of a Delta Wing at Supersonic Speeds. Quart. Appl. Math., vol. 4, no. 3, Oct. 1946, pp. 246-254.

4. Evvard, John C., and Turner, Richard L.: Theoretical Lift Distribution and Upwash Velocities for Thin Wings at Supersonic Speeds. NACA TN No. 1484, 1947.

5. Van Dyke, Milton D.: Aerodynamic Characteristics Including Scale Effect of Several Wings and Bodies Alone and in Combination at a Mach Number of 1.53. NACA RM No. A6K22, 1946.

6. Jones, R.T., and Ames, Milton B.: Wind-Tunnel Investigation of Control Surface Characteristics. V - The Use of a Beveled Trailing Edge to Reduce the Hinge Moment of a Control Surface. NACA ARR Mar. 1942.

[redacted]

7. Lindsey, W.F., Daley, Bernard N., and Humphreys, Milton D.: The Flow and Force Characteristics of Supersonic Airfoils at High Subsonic Speeds. NACA TN No. 1211, 1947.

8. Bollay, William: A Non-Linear Wing Theory and its Application to Rectangular Wings of Small Aspect Ratio. Z.f.a.M.M. Bd. 19, Nr. 1, Feb. 1939.

9. Allen, H. Julian, Heaslet, Max A., and Nitzberg, Gerald E.: The Interaction of Boundary Layer and Compression Shock and its Effect Upon Airfoil Pressure Distributions. RM No. A7A02, 1947.

10. Vincenti, Walter G., Nielsen, Jack N., and Matteson, Frederick H.: Investigation of Wing Characteristics at a Mach Number of 1.53. I – Triangular Wings of Aspect Ratio 2. NACA RM No. A7I10, 1947.

TABLE I.– EXPERIMENTAL PRESSURE COEFFICIENTS
[$M = 1.53$; $Re = 0.48 \times 10^{6}$]

Station (percent semispan)	x/c	α = 0°		α = 1°		α = 2°		α = 4°		α = 6°		α = 8°	
		$\frac{p_u-p_o}{q_o}$	$\frac{p_l-p_o}{q_o}$	$\frac{p_u-p_o}{q_o}$	$\frac{p_l-p_o}{q_o}$	$\frac{p_u-p_o}{q_o}$	$\frac{p_l-p_o}{q_o}$	$\frac{p_u-p_o}{q_o}$	$\frac{p_l-p_o}{q_o}$	$\frac{p_u-p_o}{q_o}$	$\frac{p_l-p_o}{q_o}$	$\frac{p_u-p_o}{q_o}$	$\frac{p_l-p_o}{q_o}$
6.4	0.075	0.0850	0.0930	0.0918	0.1473	0.0763	0.1878	0.0238	0.2028	0.0063	0.2508	0.0063	0.2518
	.30	.0190	.0190	.0214	.0514	–.0066	.0689	–.0236	.0994	–.0516	.1479	–.0906	.1519
	.50	–.0300	–.0300	–.0314	.0006	–.0664	.0036	–.0784	.0341	–.0984	.0791	–.1064	.1016
	.70	–.0800	–.0800	–.0715	–.0425	–.1105	–.0515	–.1125	–.0100	–.1310	.0310	–.1300	.0460
	.90	–.1130	–.1130	–.0945	–.0905	–.1255	–.1135	–.1285	–.0835	–.1705	–.0465	–.1250	–.0335
	.95	–.1100	–.1100	–.0847	–.0847	–.1257	–.1132	–.1197	–.0987	–.0842	–.0747	–.1157	–.0792
25.6	.05	.1050	.1050	.0873	.1428	.0638	.1933	–.0797	.2103	–.2097	.2573	–.2257	.2628
	.10	.0820	.0820	.0558	.1058	.0348	.1443	–.0722	.1698	–.1597	.2128	–.2602	.2278
	.30	–.0210	–.0210	–.0358	.0062	–.0688	.0237	–.0838	.0637	–.1078	.1087	–.1163	.1412
	.50	–.1000	–.0900	–.1035	–.0715	–.1405	–.0710	–.1450	–.0180	–.1735	.0225	–.1460	.0515
	.75	–.1250	–.1250	–.1108	–.1298	–.1408	–.1528	–.1358	–.1098	–.2138	–.0738	–.1523	–.0438
	.85	–.1100	–.1100	–.1018	–.1078	–.1268	–.1428	–.0868	–.1148	–.1028	–.0823	–.0943	–.0723
	.90	–.1040	–.1040	–.1037	–.1002	–.1402	–.1127	–.0702	–.0917	–.0837	–.0717	–.0732	–.0562
	.95	–.1040	–.1040	–.1116	–.0996	–.1386	–.1136	–.0616	–.0791	–.0641	–.0541	–.0676	–.0541
51.2	.10	.0310	.0310	.0200	.0740	–.0110	.1135	–.1590	.1510	–.2760	.1985	–.2830	.2205
	.20	–.0140	–.0110	–.0294	.0191	–.0594	.0421	–.1019	.0806	–.1844	.1326	–.2774	.1731
	.40	–.1020	–.1020	–.1093	–.0703	–.1510	–.0643	–.1603	–.0113	–.1923	.0322	–.1803	.0847
	.60	–.1260	–.1260	–.0832	–.1032	–.0857	–.1157	–.1722	–.0517	–.2107	–.0322	–.1417	.0233
	.70	– – –	– – –	–.0840	–.0880	–.0960	–.1050	–.1260	–.0570	–.0960	–.0650	–.0960	–.0170
	.80	–.1060	–.1060	–.0960	–.0940	–.1175	–.1100	–.0060	–.0560	–.0855	–.0890	–.0280	–.0465
	.90	–.0970	–.0970	–.0875	–.0915	–.1135	–.1080	–.0665	–.0455	–.0620	–.0770	–.0875	–.0630
76.9	.05	.0620	.0700	.0194	.1024	–.0356	.1554	–.2286	.1864	–.3786	.2179	–.2956	.2404
	.15	.0130	.0130	–.0260	.0365	–.0575	.0765	–.1650	.1125	–.2635	.1550	–.3135	.1875
	.30	–.0800	–.0750	–.0993	–.0443	–.1373	–.0263	–.1623	.0212	–.2178	.0647	–.2733	.1047
	.40	–.1270	–.1100	–.1285	–.0895	–.1560	–.0720	–.2175	.0115	–.2465	.0215	–.2510	.0925
	.50	–.1250	–.1080	–.1092	–.1222	–.1072	–.0942	–.2262	–.0647	–.2237	–.0287	–.1412	.0388
	.60	–.1060	–.1060	–.0940	–.1240	–.0875	–.1415	–.1880	–.0770	–.1120	–.0695	–.0655	–.0125
	.70	–.0970	–.0970	–.0921	–.1021	–.0931	–.1341	–.1246	–.0671	–.0656	–.0996	–.0836	–.0436
	.80	–.0900	–.0900	–.0916	–.0916	–.1156	–.0966	–.0746	–.0576	–.0471	–.1106	–.0876	–.0356
	.90	–.0990	–.0810	–.0950	–.0865	–.1300	–.0795	–.0490	–.0400	–.0630	–.1010	–.1110	–.0620
97.5	.10	0	0	–.0227	.0453	–.0542	.0743	–.2177	.1233	–.3767	.1653	–.3137	.2933
	.20	–.0600	–.0600	–.0774	–.0354	–.1149	–.0364	–.2064	.0106	–.3654	.0441	.8866	.0826
	.30	–.1100	–.1100	–.1154	– – –	–.1264	– – –	–.1694	– – –	–.3564	– – –	–.2309	– – –
	.40	–.1300	–.1200	–.1135	–.1185	–.1110	–.1035	–.2490	–.1410	–.3510	–.0760	–.2260	–.0610
	.55	–.0800	–.0700	–.0685	– – –	–.0685	– – –	–.2040	– – –	–.2815	– – –	–.1560	– – –
	.70	–.0660	–.0660	–.0530	–.0620	–.0430	–.0670	–.1460	–.0710	–.1740	–.1260	–.1220	–.0680
	.85	–.0350	–.0200	–.0210	–.0210	.0050	–.0200	–.0700	–.0020	–.0850	–.0600	–.0450	.0130

TABLE I.– CONCLUDED

[$M = 1.53$; $Re = 3.0\times10^6$]

Station (percent semispan)	x/c	$\alpha = 0^\circ$		$\alpha = 1^\circ$		$\alpha = 2^\circ$		$\alpha = 4^\circ$		$\alpha = 6^\circ$		$\alpha = 8^\circ$		$\alpha = 10^\circ$	
		$\frac{p_u-p_o}{q_o}$	$\frac{p_l-p_o}{q_o}$	$\frac{p_u-p_o}{q_o}$	$\frac{p_l-p_o}{q_o}$	$\frac{p_u-p_o}{q_o}$	$\frac{p_l-p_o}{q_o}$	$\frac{p_u-p_o}{q_o}$	$\frac{p_l-p_o}{q_o}$	$\frac{p_u-p_o}{q_o}$	$\frac{p_l-p_o}{q_o}$	$\frac{p_u-p_o}{q_o}$	$\frac{p_l-p_o}{q_o}$	$\frac{p_u-p_o}{q_o}$	$\frac{p_l-p_o}{q_o}$
6.4	0.075	0.0935	0.1165	0.0775	0.1895	0.0575	0.2490	0.0290	– – –	-0.0015	0.2365	-0.0210	0.2785	-0.0250	0.3190
	.30	.0335	.0475	.0145	.0615	-.0035	.0765	-.0295	.1180	-.0525	.1585	-.0750	.2035	-.1010	.2475
	.50	-.0227	-.0117	-.0337	-.0007	-.0467	.0123	-.0732	.0493	-.0977	.0838	-.1207	.1248	-.1407	.1633
	.70	-.0693	-.0573	-.0833	-.0453	-.0953	-.0338	-.1188	.0002	-.1408	.0297	-.1593	.0667	-.1753	.1027
	.90	-.1080	-.0980	-.1180	-.0920	-.1270	-.0820	-.1405	-.0505	-.1565	-.0245	-.1710	.0065	-.1820	.0380
	.95	-.0365	-.0605	-.0405	-.0635	-.0400	-.0665	-.0440	-.0665	-.0530	-.0620	-.0655	-.0505	-.0765	-.0345
25.6	.05	.1110	.1190	.0850	.1460	.0595	.1685	-.0590	.2185	-.2085	.2560	-.2795	.2985	-.3260	.3430
	.10	.0805	.0915	.0585	.1125	.0415	.1325	-.0105	.1785	-.1705	.2175	-.2840	.2615	-.3445	.3055
	.30	-.0160	-.0070	-.0350	.0090	-.0440	.0310	-.0800	.0640	-.1050	.1190	-.1010	.1615	-.2660	.2015
	.50	-.0662	-.0602	-.0842	-.0492	-.0972	-.0352	-.1292	.0043	-.1522	.0388	-.1692	.0808	-.1682	.1213
	.75	-.1388	-.1218	-.1518	-.1088	-.1578	-.0968	-.1758	-.0643	-.1918	-.0383	-.2093	-.0018	-.2283	.0322
	.85	-.0707	-.0757	-.0747	-.0787	-.0552	-.0842	-.0567	-.0832	-.0612	-.0682	-.0607	-.0462	-.0597	-.0242
	.90	-.0599	-.0329	-.0579	-.0339	-.0384	-.0494	-.0454	-.0604	-.0524	-.0604	-.0539	-.0514	-.0524	-.0399
	.95	-.0040	-.0030	0	0	-.0080	-.0160	-.0270	-.0400	-.0440	-.0475	-.0510	-.0490	-.0555	-.0460
51.2	.10	.0530	.590	.0210	.0840	-.0045	.1070	-.1150	.1600	-.2370	.1945	-.3260	.2360	-.3705	.2750
	.20	.0002	.0172	-.0238	.0272	-.0438	.0497	-.0903	.1042	-.2068	.1422	-.3148	.1832	-.3738	.2182
	.40	-.0835	-.0765	-.1045	-.0625	-.1210	-.0415	-.1585	.0035	-.1875	.0375	-.2795	.0805	-.3665	.1210
	.60	-.1385	-.1365	-.1605	-.1195	-.1805	-.1020	-.2090	-.0610	-.2265	-.0285	-.2445	.0080	-.3290	.0410
	.70	-.1749	-.1690	-.1970	-.1590	-.1265	-.1475	-.0910	-.1145	-.1055	-.0860	-.1760	-.0550	-.3020	-.0265
	.80	-.0430	-.0490	-.0430	-.0550	-.0280	-.0795	-.0420	-.0885	-.0695	-.0820	-.1130	-.0645	-.2110	-.0410
	.90	-.0048	-.0038	-.0018	-.0088	-.0113	-.0363	-.0438	-.0603	-.0743	-.0643	-.0793	-.0518	-.0218	-.0368
76.9	.05	.0570	.0440	.0190	.1050	-.0175	.1305	-.2755	.1755	-.3560	.2025	-.3915	.2315	-.4115	.2540
	.15	-.0020	.0080	-.0330	.0320	-.0585	.0545	-.1490	.1050	-.2990	.1460	-.3765	.1865	-.4200	.2210
	.30	-.0777	-.0787	-.1047	-.0537	-.1237	-.0292	-.1707	.0178	-.2467	.0583	-.3427	.0988	-.3972	.1353
	.40	-.1165	-.1085	-.1335	-.1015	-.1560	-.0810	-.2010	-.0340	-.2380	.0030	-.2860	.0415	-.3615	.0810
	.50	-.1470	-.1390	-.1670	-.1170	-.1865	-.0980	-.2260	-.0510	-.1860	-.0140	-.2510	.0255	-.3480	.0589
	.60	-.1828	-.1838	-.1968	-.1628	-.1583	-.1483	-.0938	-.1038	-.1153	-.0703	-.2413	-.0358	-.3478	-.0008
	.70	-.0926	-.0946	-.0926	-.0936	-.0486	-.1146	-.0466	-.1111	-.0801	-.0901	-.2376	-.0631	-.3576	-.0326
	.80	-.0460	-.0520	-.0370	-.0600	-.0235	-.0960	-.0330	-.1140	-.0775	-.1045	-.2390	-.0765	-.3745	-.0420
	.90	-.0125	-.0065	-.0055	-.0145	-.0175	-.0470	-.0375	-.0860	-.0980	-.0915	-.2020	-.0715	-.2905	-.0380
97.5	.10	.0155	.0275	-.0085	.0505	-.0370	.0760	-.2150	.1275	-.3665	.1700	-.3865	.2075	-.3505	.2385
	.20	-.0538	-.0478	-.0748	-.0318	-.0938	-.0178	-.1543	.0122	-.3258	.0477	-.3798	.0802	-.3178	.1127
	.30	-.1040	– – –	-.1210	– – –	-.1405	– – –	.1700	– – –	-.3310	– – –	-.3645	– – –	.2885	– – –
	.40	-.1404	-.1384	-.1554	-.1274	-.1749	-.1134	-.2139	-.1059	-.3114	-.0864	-.3424	-.0629	-.2754	-.0364
	.55	-.1899	– – –	-.2079	– – –	-.1449	– – –	-.1489	– – –	-.2424	– – –	-.2814	– – –	-.2199	– – –
	.70	-.0700	-.0820	-.0590	-.0930	-.0275	-.1215	-.1100	-.1385	-.1780	-.1380	-.2625	-.1130	-.1830	-.0880
	.85	-.0015	-.0125	.0085	-.0315	.0085	-.0530	-.0870	-.0720	-.1500	-.0940	-.2400	-.1095	-.0935	-.1095

NACA

TABLE I.– CONCLUDED

[$M = 1.53$; $Re = 3.0 \times 10^6$]

Station (percent semispan)	x/c	α = 0°		α = 1°		α = 2°		α = 4°		α = 6°		α = 8°		α = 10°	
		$\frac{p_u-p_o}{q_o}$	$\frac{p_l-p_o}{q_o}$	$\frac{p_u-p_o}{q_o}$	$\frac{p_l-p_o}{q_o}$	$\frac{p_u-p_o}{q_o}$	$\frac{p_l-p_o}{q_o}$	$\frac{p_u-p_o}{q_o}$	$\frac{p_l-p_o}{q_o}$	$\frac{p_u-p_o}{q_o}$	$\frac{p_l-p_o}{q_o}$	$\frac{p_u-p_o}{q_o}$	$\frac{p_l-p_o}{q_o}$	$\frac{p_u-p_o}{q_o}$	$\frac{p_l-p_o}{q_o}$
6.4	0.075	0.0935	0.1165	0.0775	0.1895	0.0575	0.2490	0.0290	– – –	-0.0015	0.2365	–0.0210	0.2785	–0.0250	0.3190
	.30	.0335	.0475	.0145	.0615	–.0035	.0765	–.0295	.1180	–.0525	.1585	–.0750	.2035	–.1010	.2475
	.50	–.0227	–.0117	–.0337	–.0007	–.0467	.0123	–.0732	.0493	–.0977	.0838	–.1207	.1248	–.1407	.1633
	.70	–.0693	–.0573	–.0833	–.0453	–.0953	–.0338	–.1188	.0002	–.1408	.0297	–.1593	.0667	–.1753	.1027
	.90	–.1080	–.0980	–.1180	–.0920	–.1270	–.0820	–.1405	–.0505	–.1565	–.0245	–.1710	.0065	–.1820	.0380
	.95	–.0365	–.0605	–.0405	–.0635	–.0400	–.0665	–.0440	–.0665	–.0530	–.0620	–.0655	–.0505	–.0765	–.0345
25.6	.05	.1110	.1190	.0850	.1460	.0595	.1685	–.0590	.2185	–.2085	.2560	–.2795	.2985	–.3260	.3430
	.10	.0805	.0915	.0585	.1125	.0415	.1325	–.0105	.1785	–.1705	.2175	–.2840	.2615	–.3445	.3055
	.30	–.0160	–.0070	–.0350	.0090	–.0440	.0310	–.0800	.0640	–.1050	.1190	–.1010	.1615	–.2660	.2015
	.50	–.0662	–.0602	–.0842	–.0492	–.0972	–.0352	–.1292	.0043	–.1522	.0388	–.1692	.0808	–.1682	.1213
	.75	–.1388	–.1218	–.1518	–.1088	–.1578	–.0968	–.1758	–.0643	–.1918	–.0383	–.2093	–.0018	–.2283	.0322
	.85	–.0707	–.0757	–.0747	–.0787	–.0552	–.0842	–.0567	–.0832	–.0612	–.0682	–.0607	–.0462	–.0597	–.0242
	.90	–.0599	–.0329	–.0579	–.0339	–.0384	–.0494	–.0454	–.0604	–.0524	–.0604	–.0539	–.0514	–.0524	–.0399
	.95	–.0040	–.0030	0	0	–.0080	–.0160	–.0270	–.0400	–.0440	–.0475	–.0510	–.0490	–.0555	–.0460
51.2	.10	.0530	.590	.0210	.0840	–.0045	.1070	–.1150	.1600	–.2370	.1945	–.3260	.2360	–.3705	.2750
	.20	.0002	.0172	–.0238	.0272	–.0438	.0497	–.0903	.1042	–.2068	.1422	–.3148	.1832	–.3738	.2182
	.40	–.0835	–.0765	–.1045	–.0625	–.1210	–.0415	–.1585	.0035	–.1875	.0375	–.2795	.0805	–.3665	.1210
	.60	–.1385	–.1365	–.1605	–.1195	–.1805	–.1020	–.2090	–.0610	–.2265	–.0285	–.2445	.0080	–.3290	.0410
	.70	–.1749	–.1690	–.1970	–.1590	–.1265	–.1475	–.0910	–.1145	–.1055	–.0860	–.1760	–.0550	–.3020	–.0265
	.80	–.0430	–.0490	–.0430	–.0550	–.0280	–.0795	–.0420	–.0885	–.0695	–.0820	–.1130	–.0645	–.2110	–.0410
	.90	–.0048	–.0038	–.0018	–.0088	–.0113	–.0363	–.0438	–.0603	–.0743	–.0643	–.0793	–.0518	–.0218	–.0368
76.9	.05	.0570	.0440	.0190	.1050	–.0175	.1305	–.2755	.1755	–.3560	.2025	–.3915	.2315	–.4115	.2540
	.15	–.0020	.0080	–.0330	.0320	–.0585	.0545	–.1490	.1050	–.2990	.1460	–.3765	.1865	–.4200	.2210
	.30	–.0777	–.0787	–.1047	–.0537	–.1237	–.0292	–.1707	.0178	–.2467	.0583	–.3427	.0988	–.3972	.1353
	.40	–.1165	–.1085	–.1335	–.1015	–.1560	–.0810	–.2010	–.0340	–.2380	.0030	–.2860	.0415	–.3615	.0810
	.50	–.1470	–.1390	–.1670	–.1170	–.1865	–.0980	–.2260	–.0510	–.1860	–.0140	–.2510	.0255	–.3480	.0589
	.60	–.1828	–.1838	–.1968	–.1628	–.1583	–.1483	–.0938	–.1038	–.1153	–.0703	–.2413	–.0358	–.3478	–.0008
	.70	–.0926	–.0946	–.0926	–.0936	–.0486	–.1146	–.0466	–.1111	–.0801	–.0901	–.2376	–.0631	–.3576	–.0326
	.80	–.0460	–.0520	–.0370	–.0600	–.0235	–.0960	–.0330	–.1140	–.0775	–.1045	–.2390	–.0765	–.3745	–.0420
	.90	–.0125	–.0065	–.0055	–.0145	–.0175	–.0470	–.0375	–.0860	–.0980	–.0915	–.2020	–.0715	–.2905	–.0380
97.5	.10	.0155	.0275	–.0085	.0505	–.0370	.0760	–.2150	.1275	–.3665	.1700	–.3865	.2075	–.3505	.2385
	.20	–.0538	–.0478	–.0748	–.0318	–.0938	–.0178	–.1543	.0122	–.3258	.0477	–.3798	.0802	–.3178	.1127
	.30	–.1040	– – –	–.1210	– – –	–.1405	– – –	.1700	– – –	–.3310	– – –	–.3645	– – –	.2885	– – –
	.40	–.1404	–.1384	–.1554	–.1274	–.1749	–.1134	–.2139	–.1059	–.3114	–.0864	–.3424	–.0629	–.2754	–.0364
	.55	–.1899	– – –	–.2079	– – –	–.1449	– – –	–.1489	– – –	–.2424	– – –	–.2814	– – –	–.2199	– – –
	.70	–.0700	–.0820	–.0590	–.0930	–.0275	–.1215	–.1100	–.1385	–.1780	–.1380	–.2625	–.1130	–.1830	–.0880
	.85	–.0015	–.0125	.0085	–.0315	.0085	–.0530	–.0870	–.0720	–.1500	–.0940	–.2400	–.1095	–.0935	–.1095

NACA

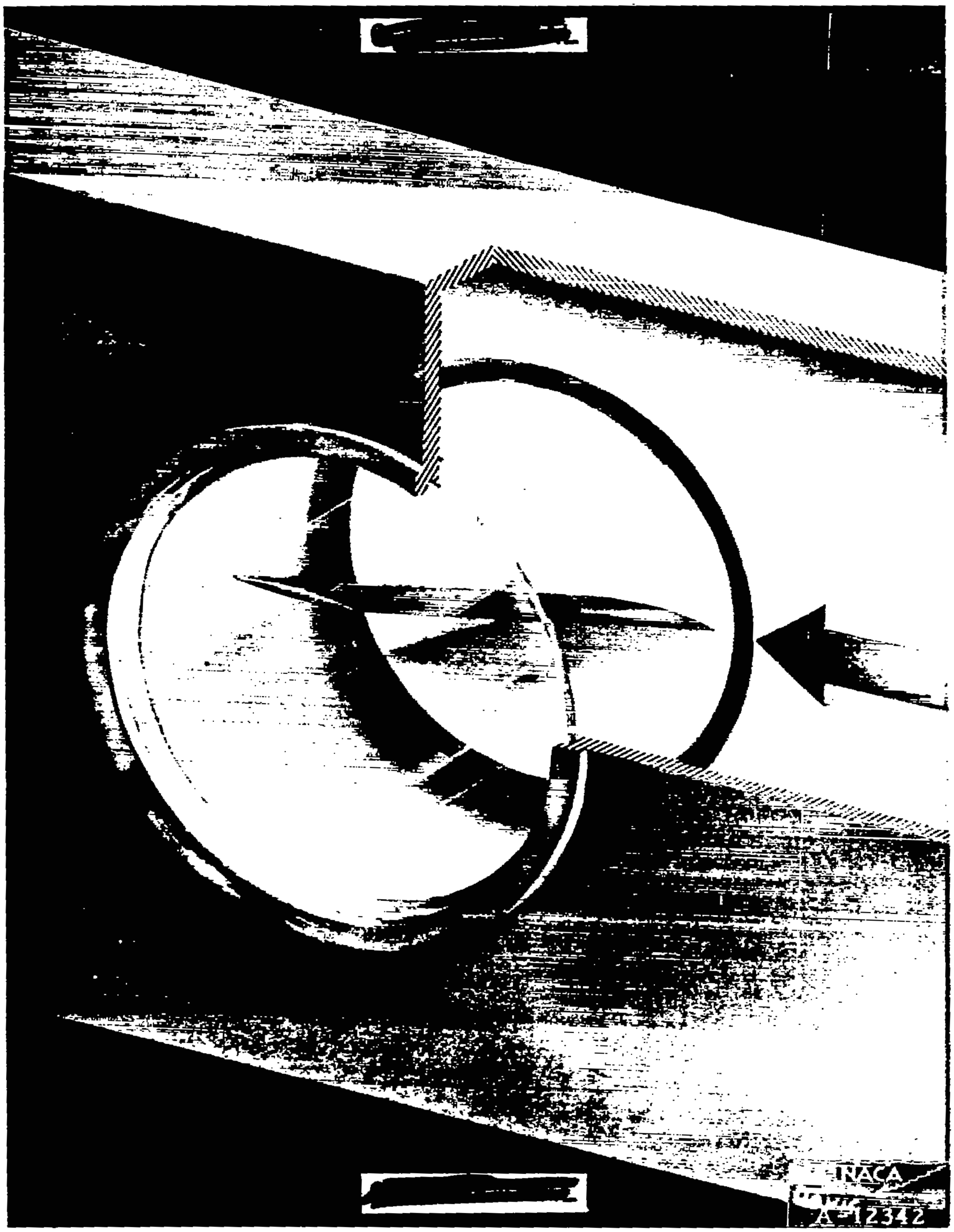
NACA
A-12342

Figure 1.— Sketch of airfoil mounted for test.

[redacted]

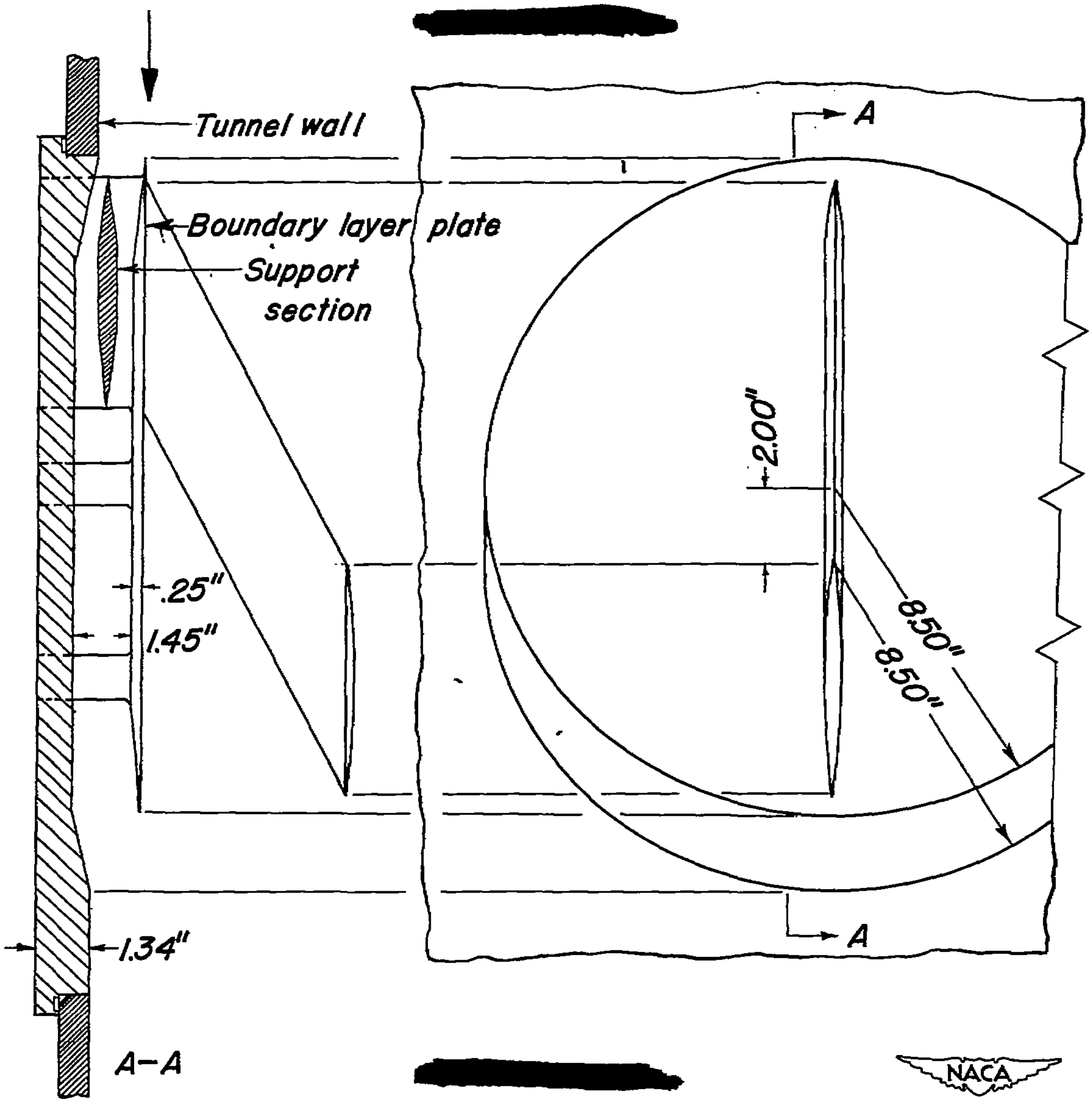
Tunnel wall
Boundary layer plate
Support section
A
A
2.00"
.25"
1.45"
8.50"
8.50"
1.34"
A–A
NACA

[redacted]

Figure 2.– Sketch of model support system.

[redacted]

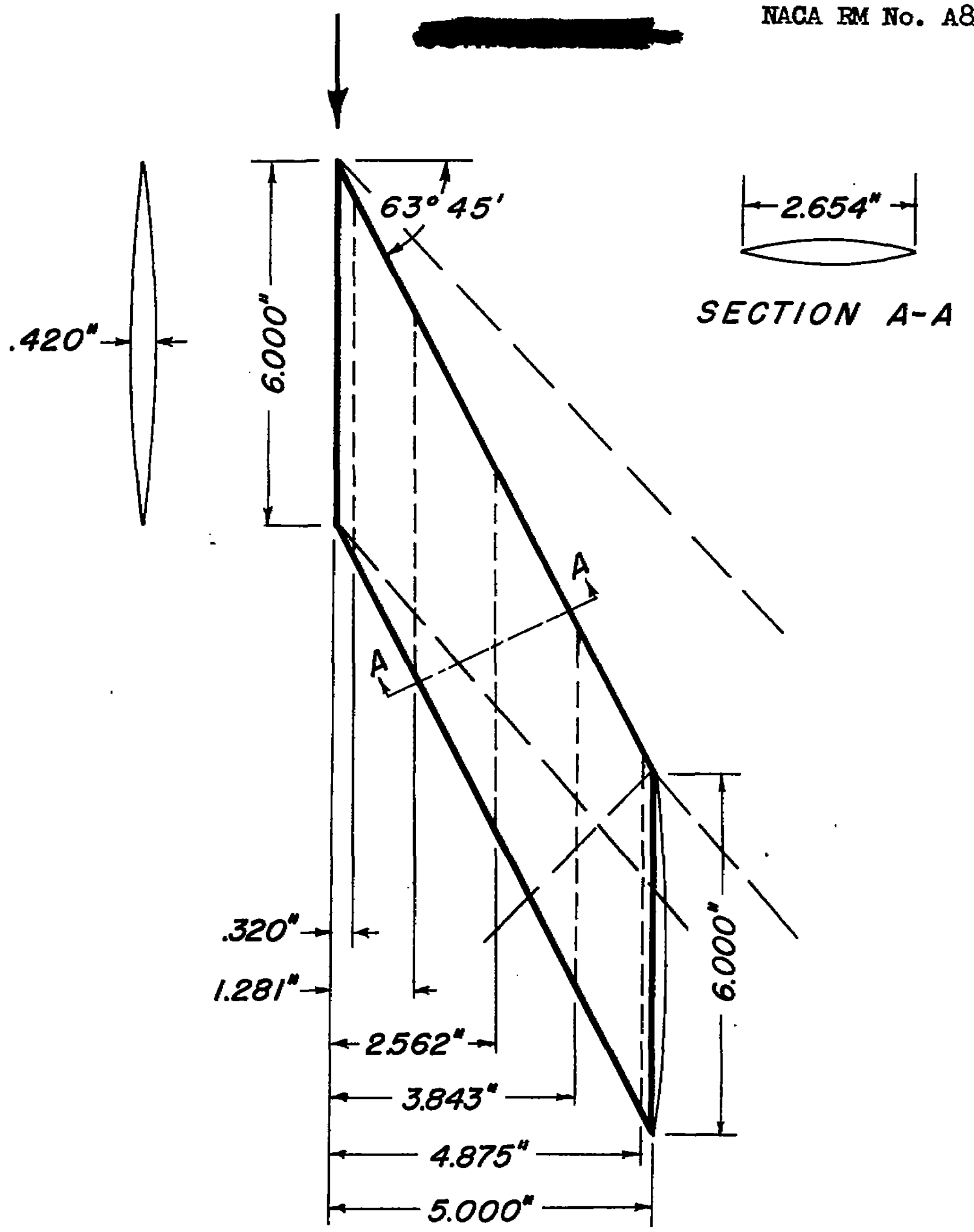
63° 45'
.420"
6.000"
2.654"
SECTION A-A
A
A
6.000"
.320"
1.281"
2.562"
3.843"
4.875"
5.000"

[redacted]

-----Pressure survey stations
— — Mach lines

Figure 3.– Dimensional sketch of model showing pressure survey stations.

[redacted]

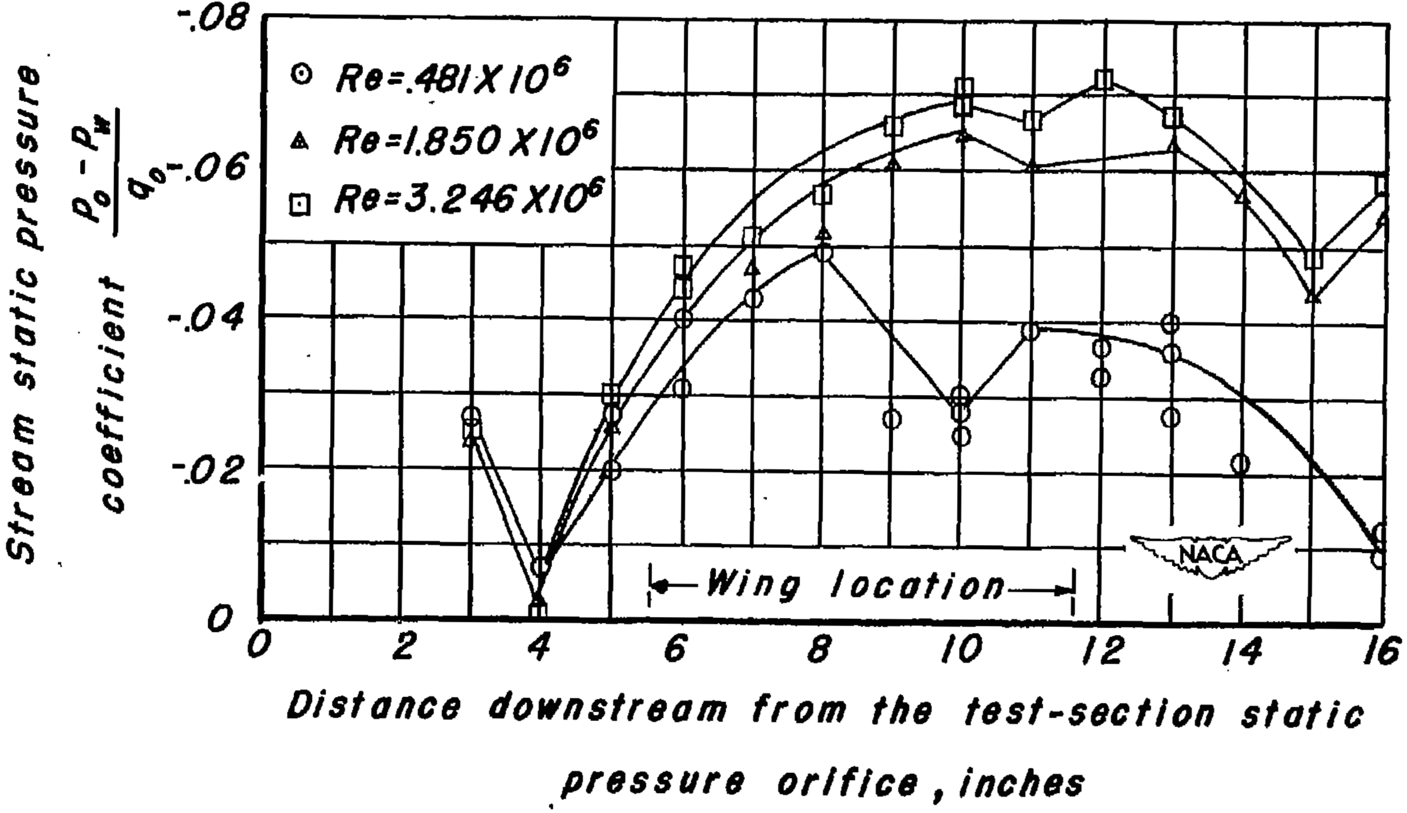

(a) 25-percent of model span from root.

Figure 4.- Axial static pressure variation in wind-tunnel stream.

[redacted]

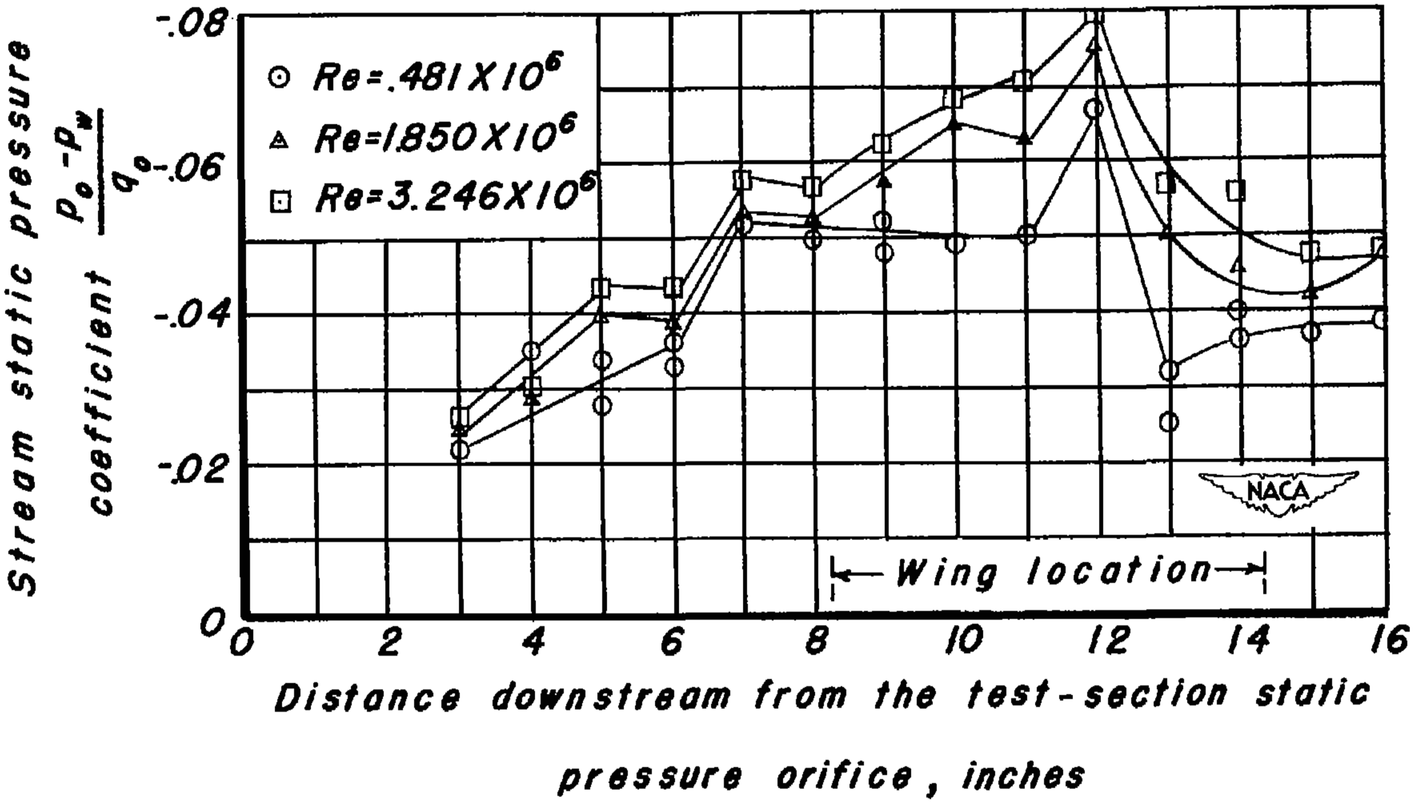

(b) 50-percent model span from root.

Figure 4.- Continued

[redacted]

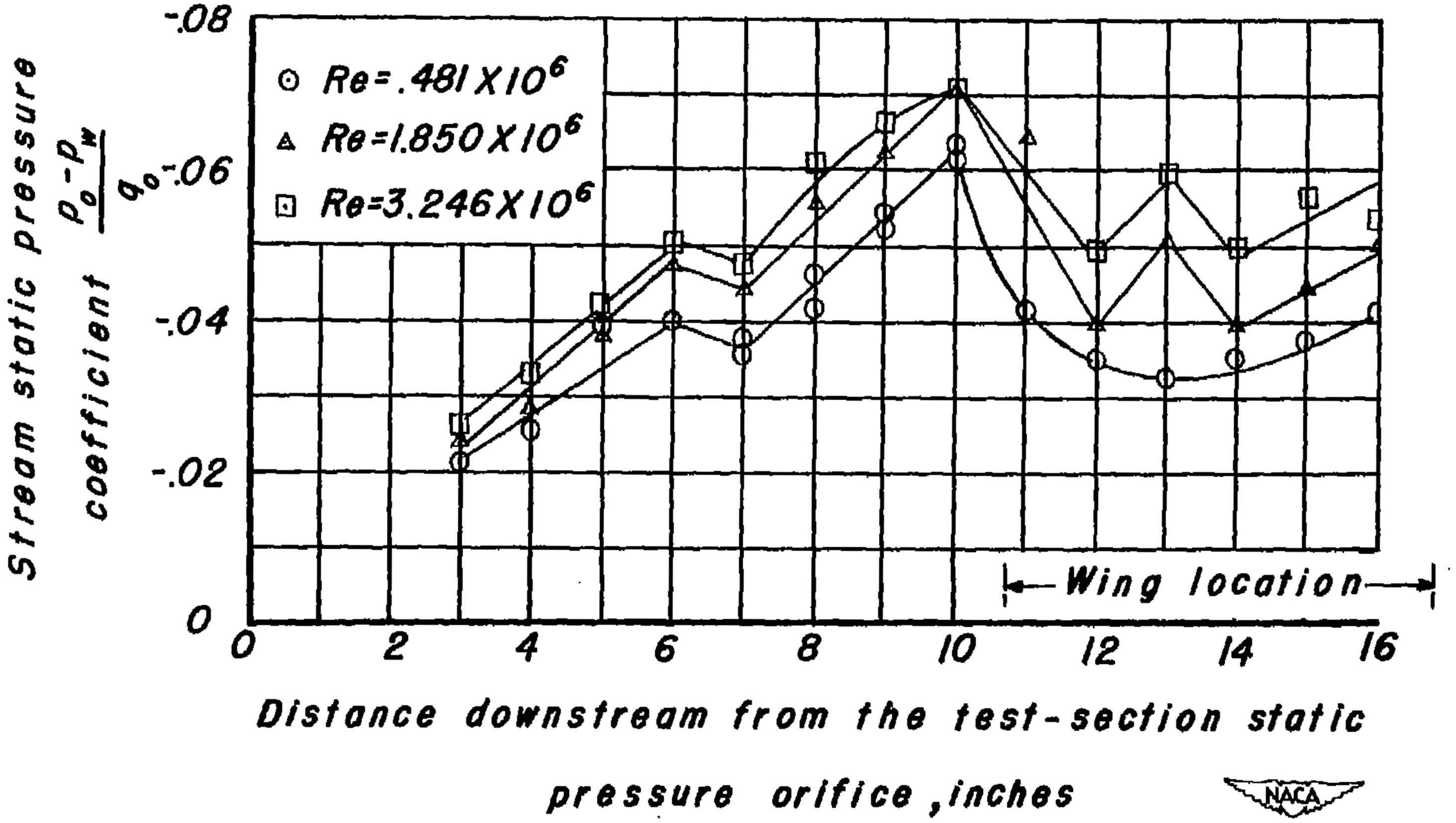

(c) 75-percent model span from root.

Figure 4.- Concluded.

[redacted]

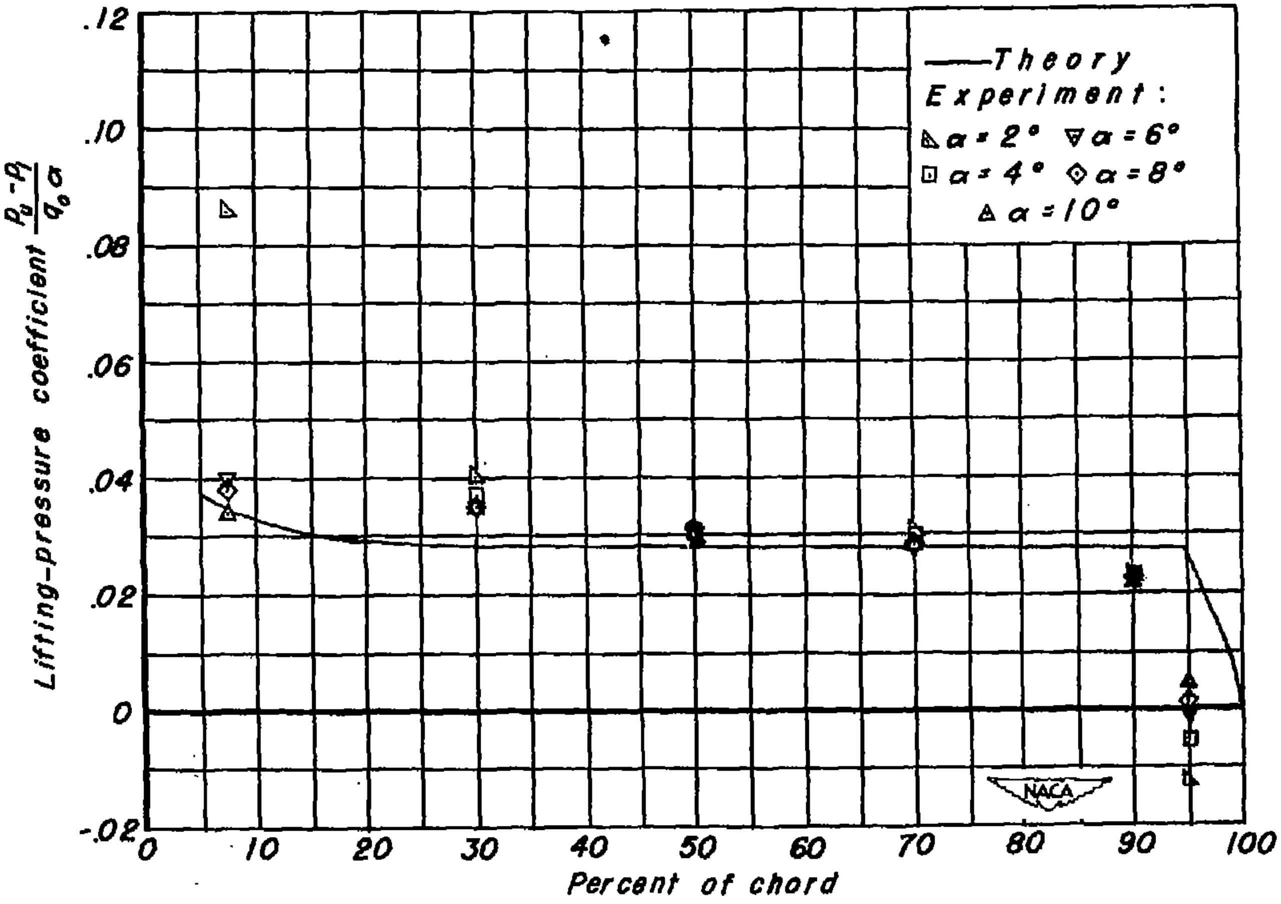

(a) 6.4% Semispan.

Figure 5.—Chordwise variation of lifting-pressure coefficient per degree angle of attack with angle of attack at five spanwise stations. Re = 3×10^6.

[redacted]

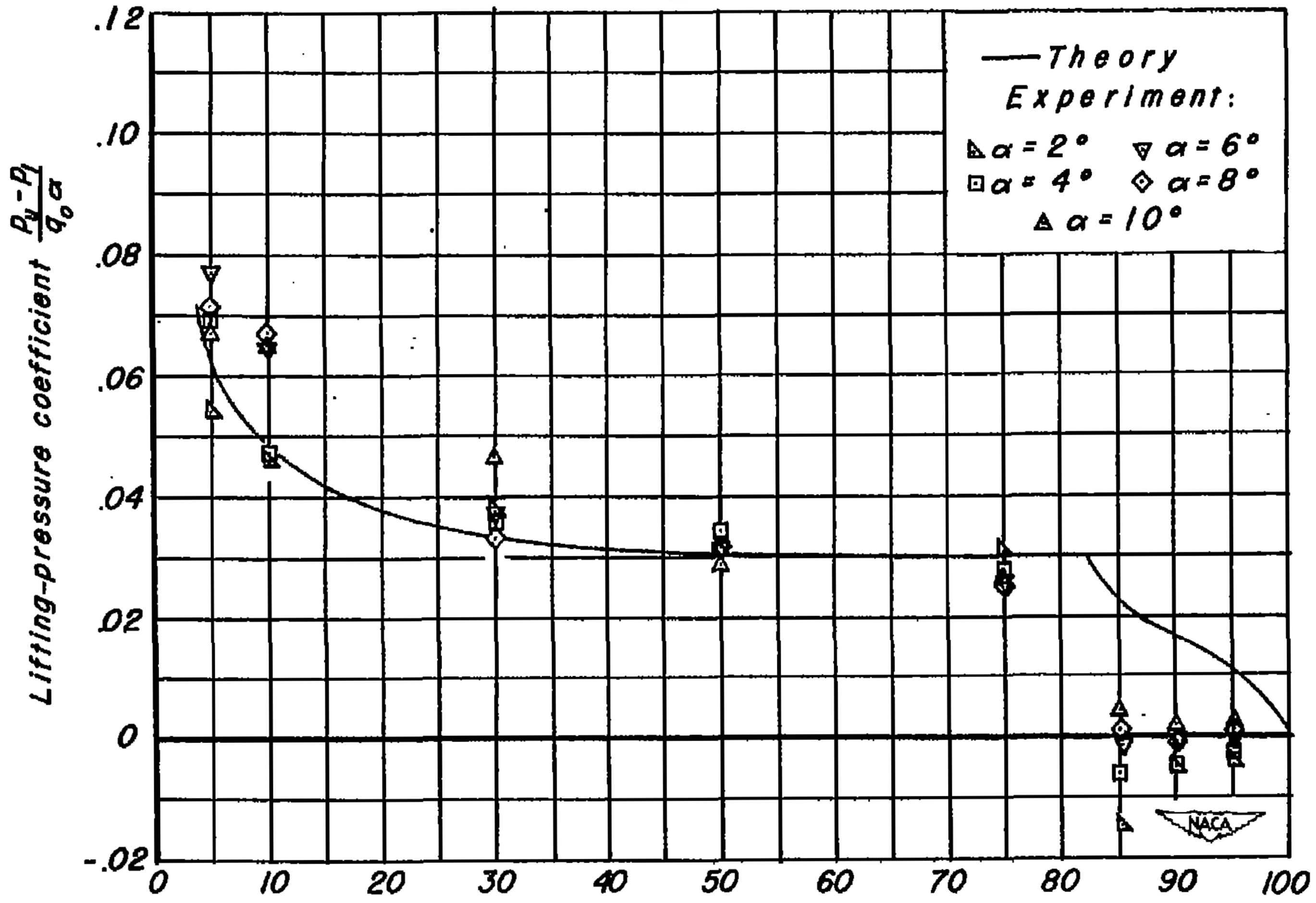

(b) 25.6 % Semispan.

Figure 5.—Continued.

[redacted]

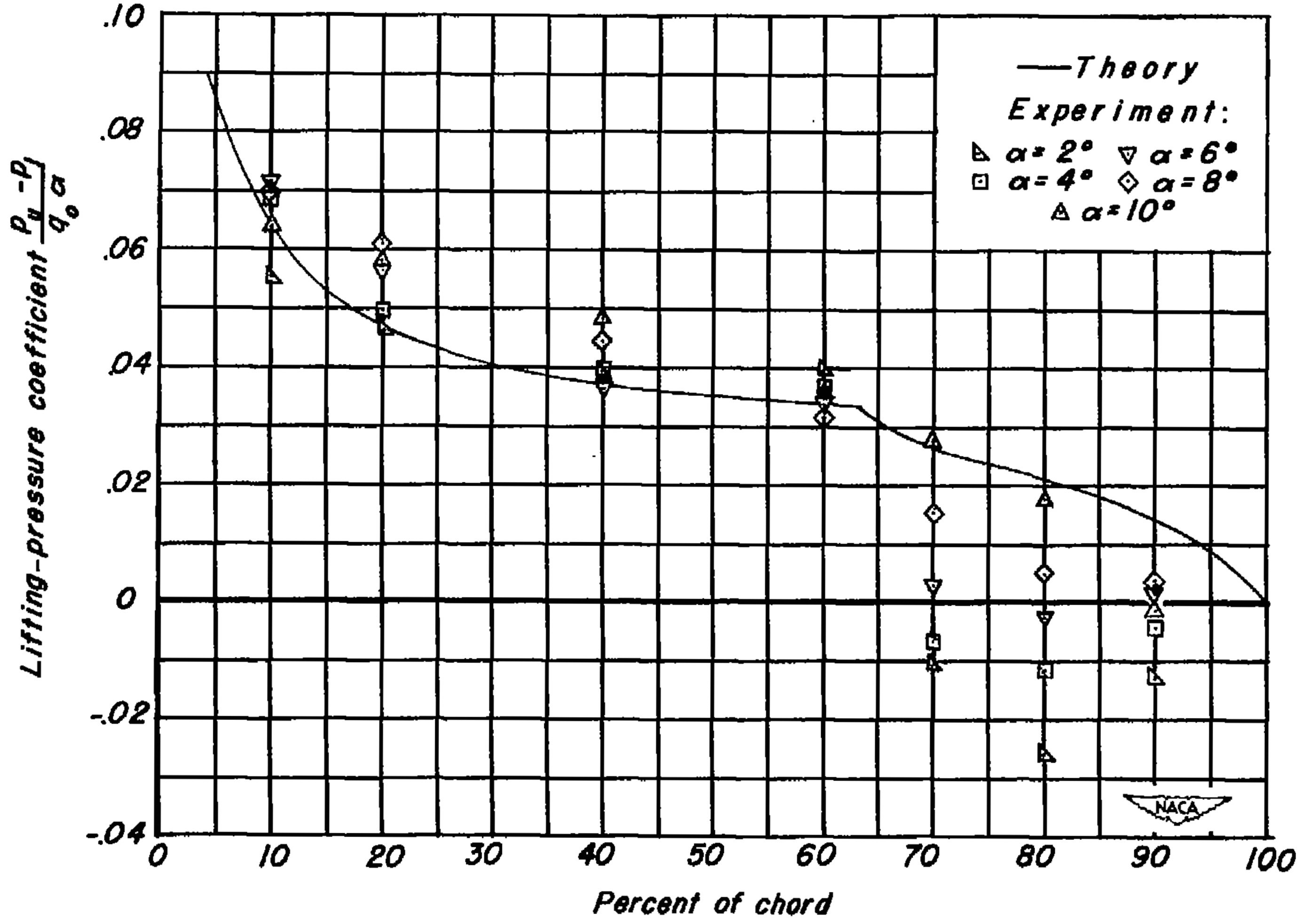

(c) 51.2% Semispan.

Figure 5.—Continued.

[redacted]

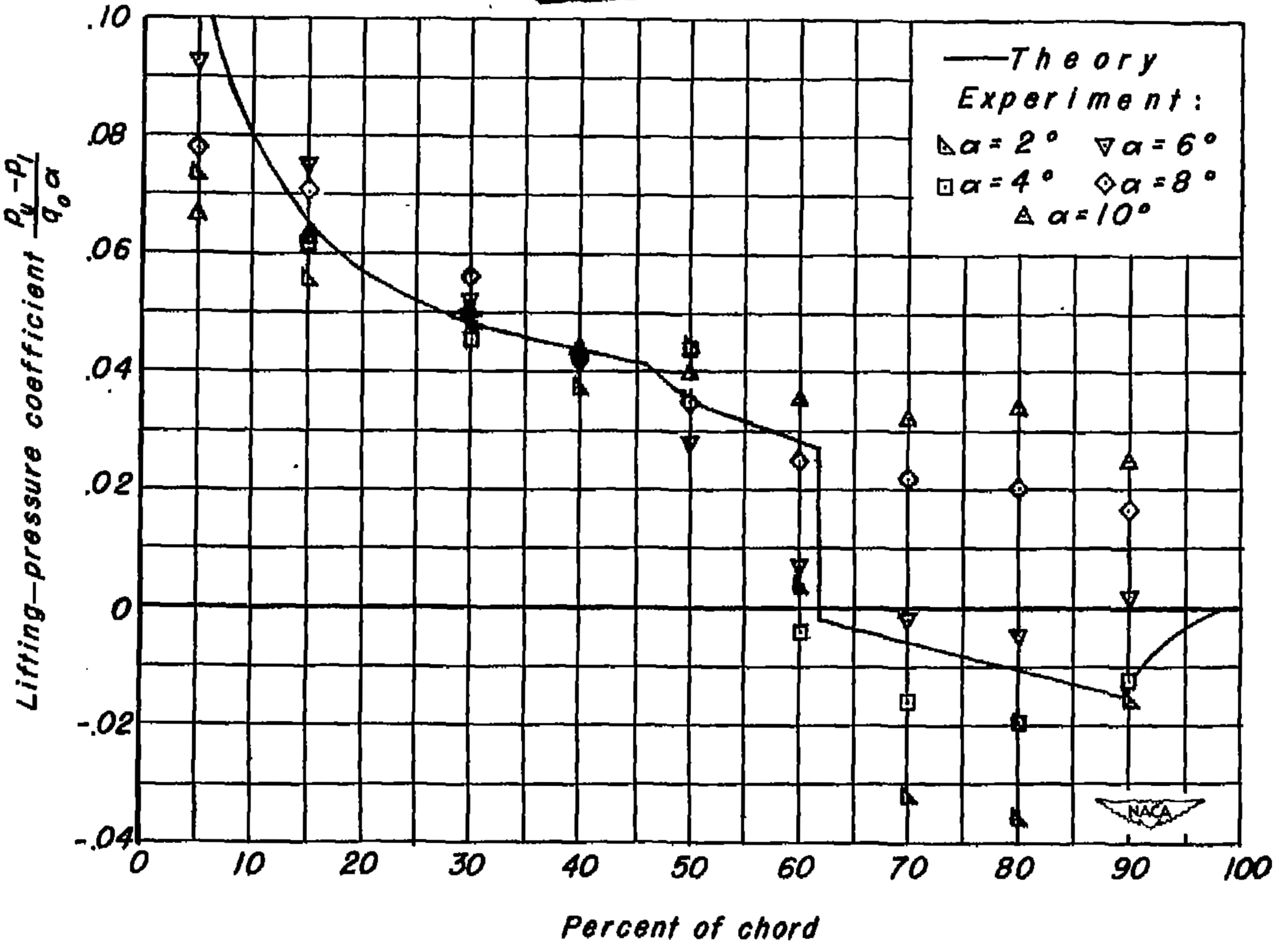

(d) 76.9% Semispan.

Figure 5.-Continued.

[redacted]

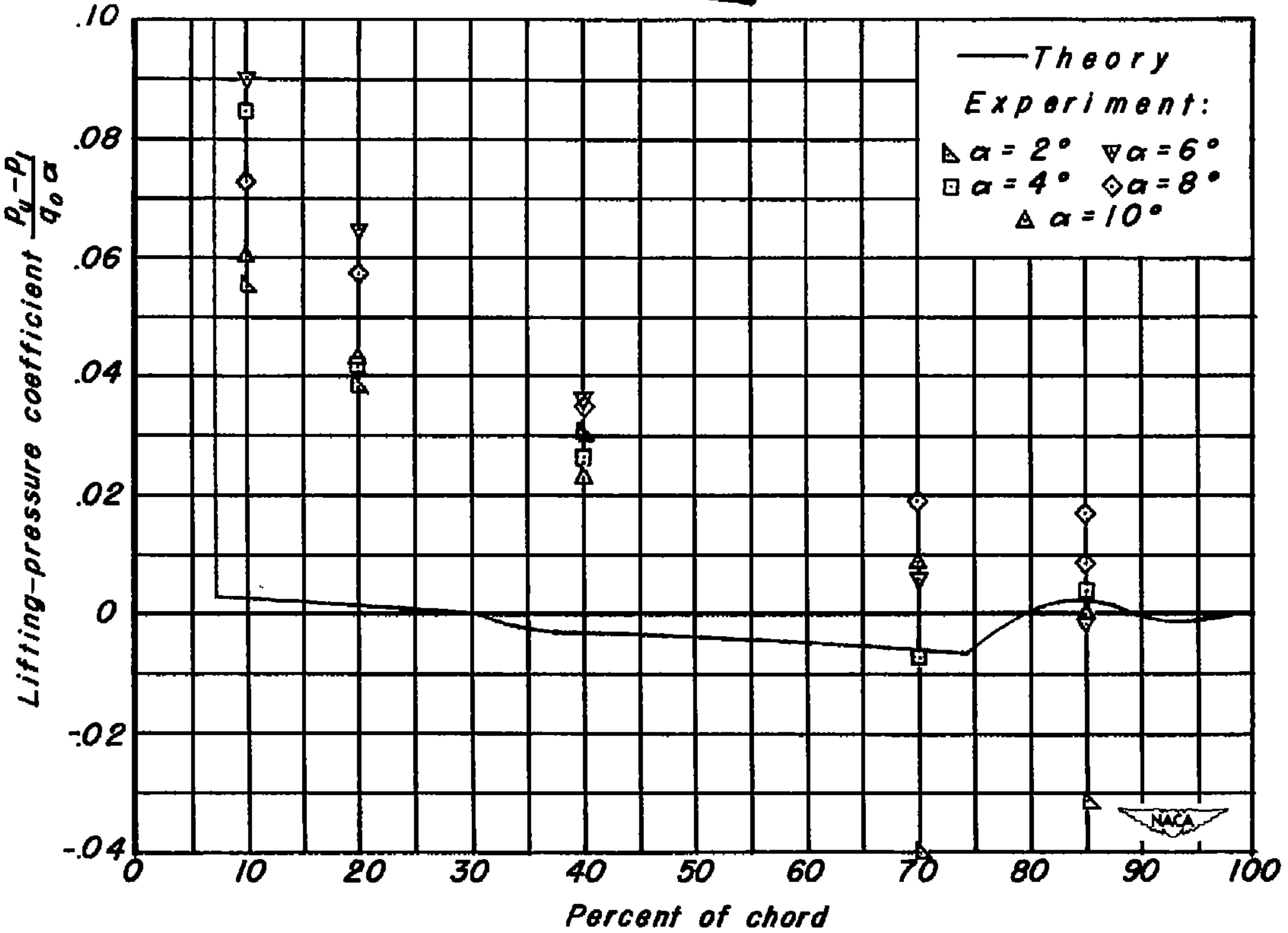

(e) 97.5 % Semispan.

Figure 5.—Concluded.

[redacted]

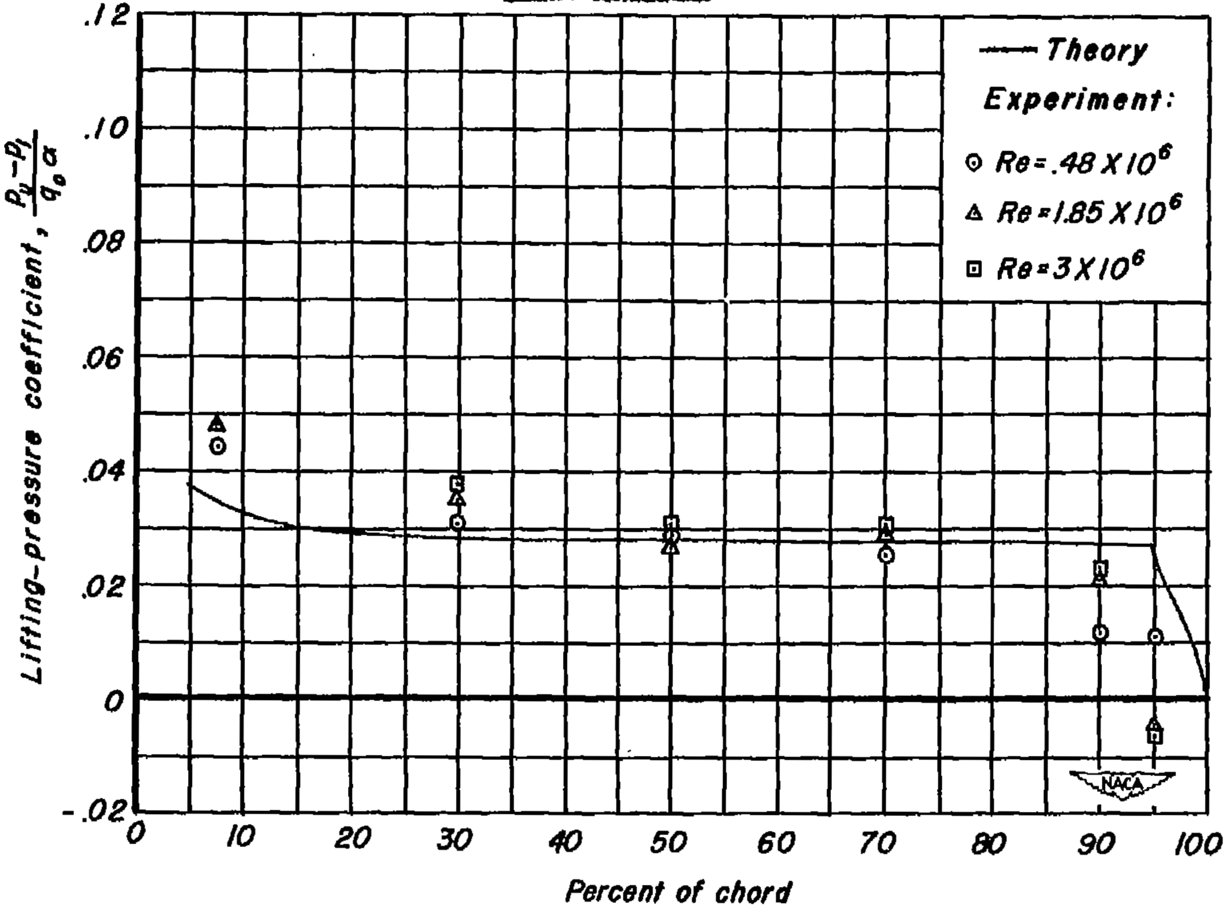

(a) 6.4% Semispan

Figure 6.— Chordwise variation of lifting-pressure coefficient per degree angle of attack with Reynolds number at five spanwise stations. $\alpha = 4°$.

[redacted]

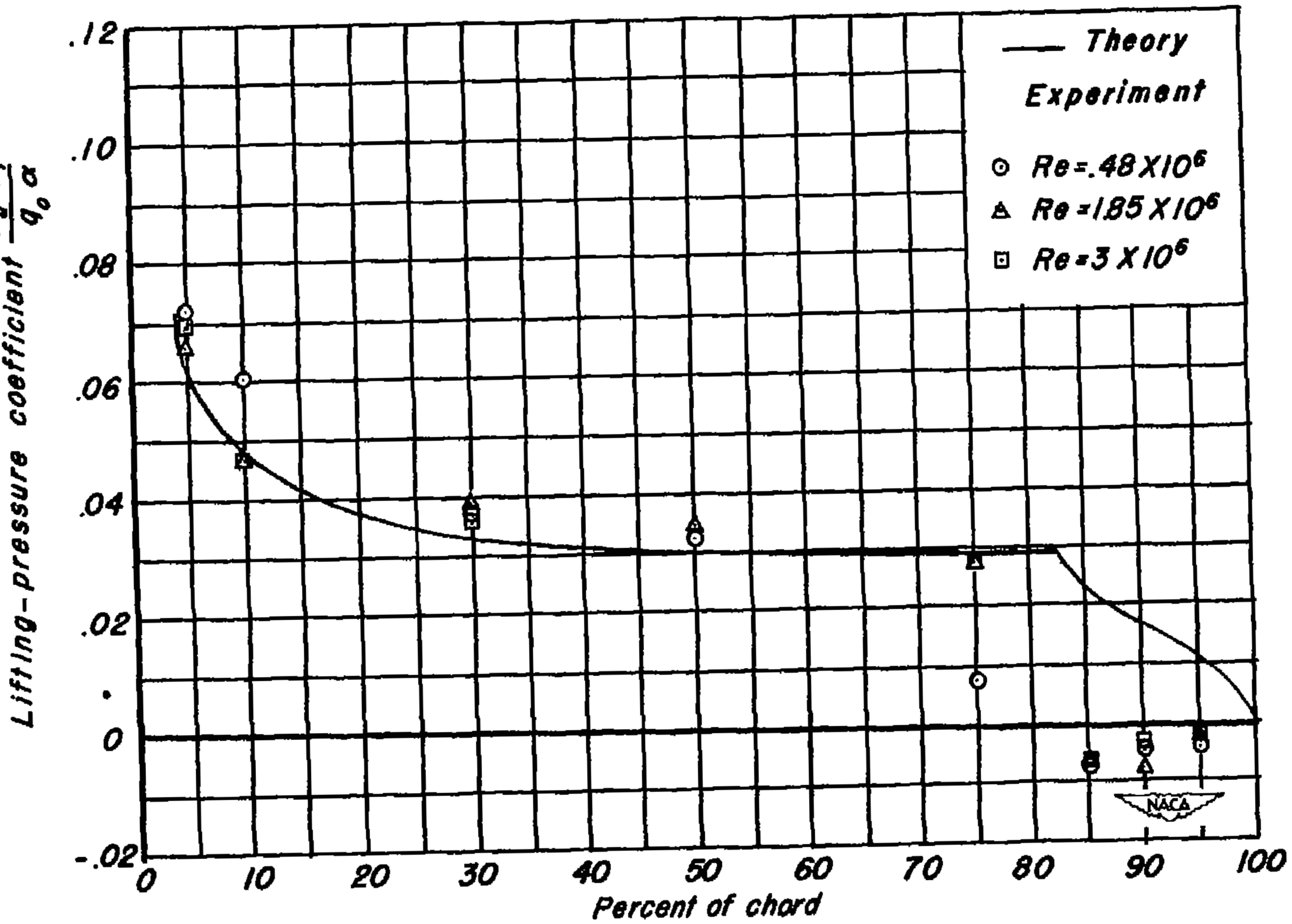

(b) 25.6% Semispan.

Figure 6.—Continued.

[redacted]

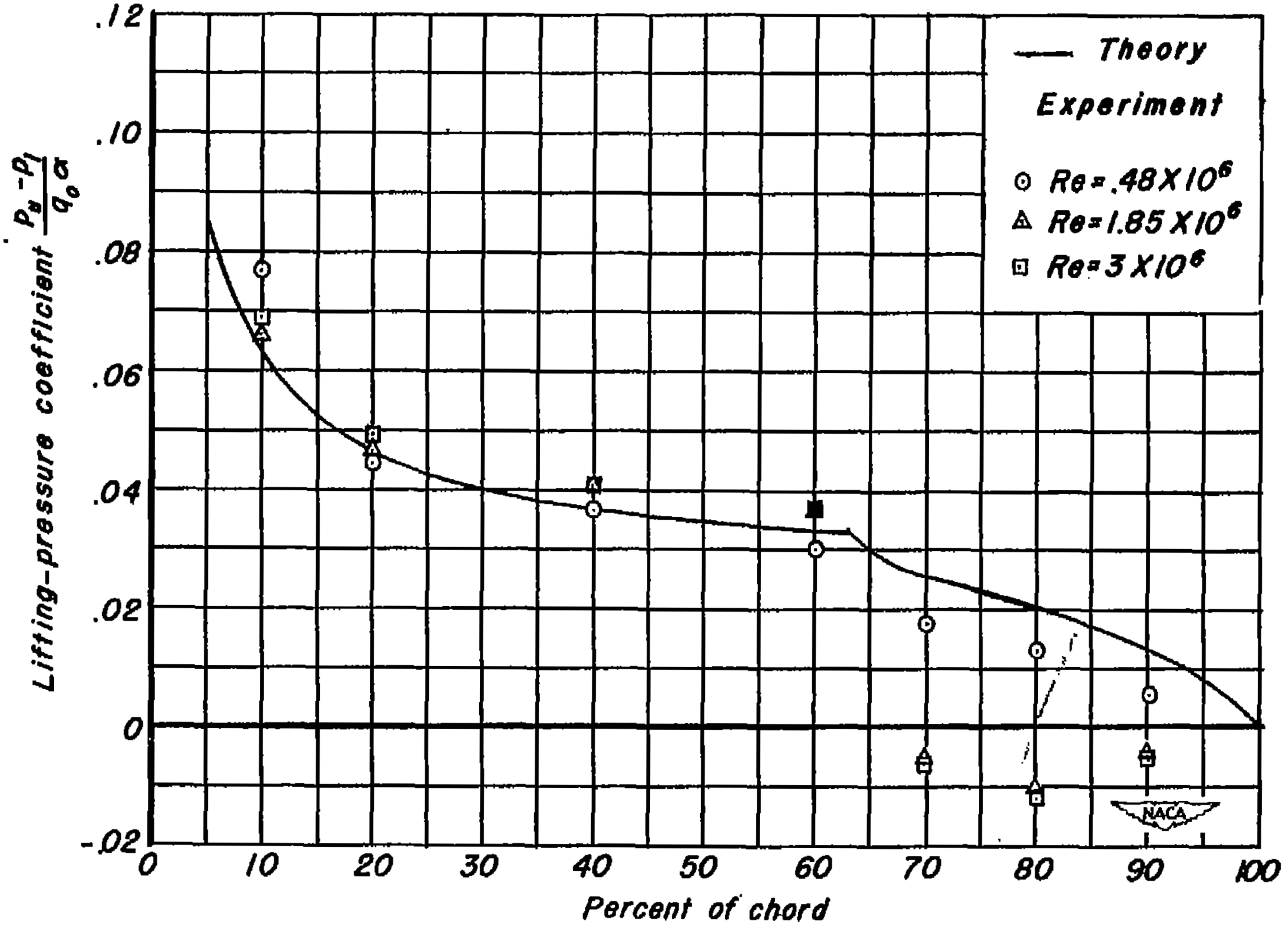

(c) 51.2% Semispan.

Figure 6.—Continued.

[redacted]

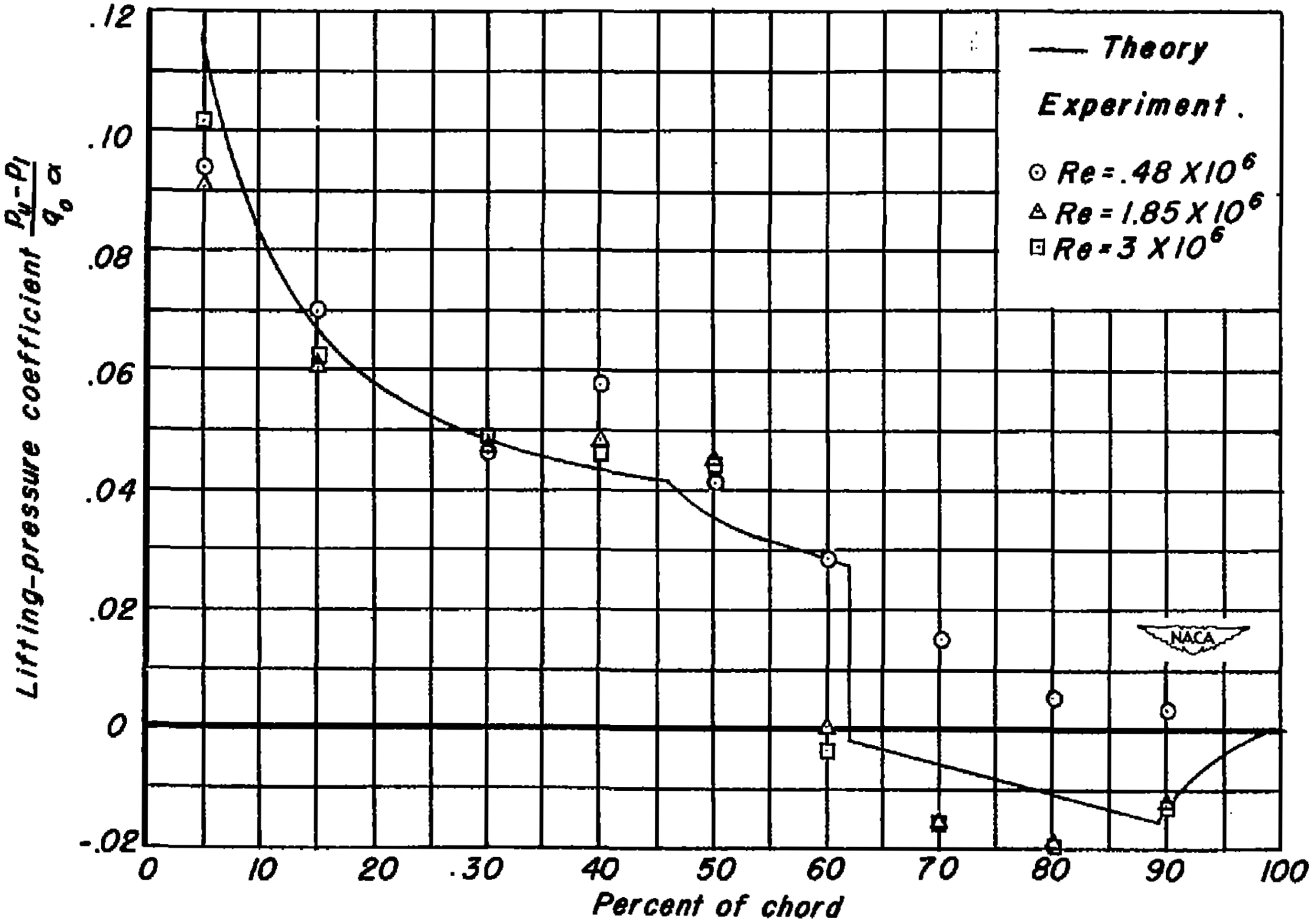

(d) 76.9% Semispan.

Figure 6.—Continued.

[redacted]

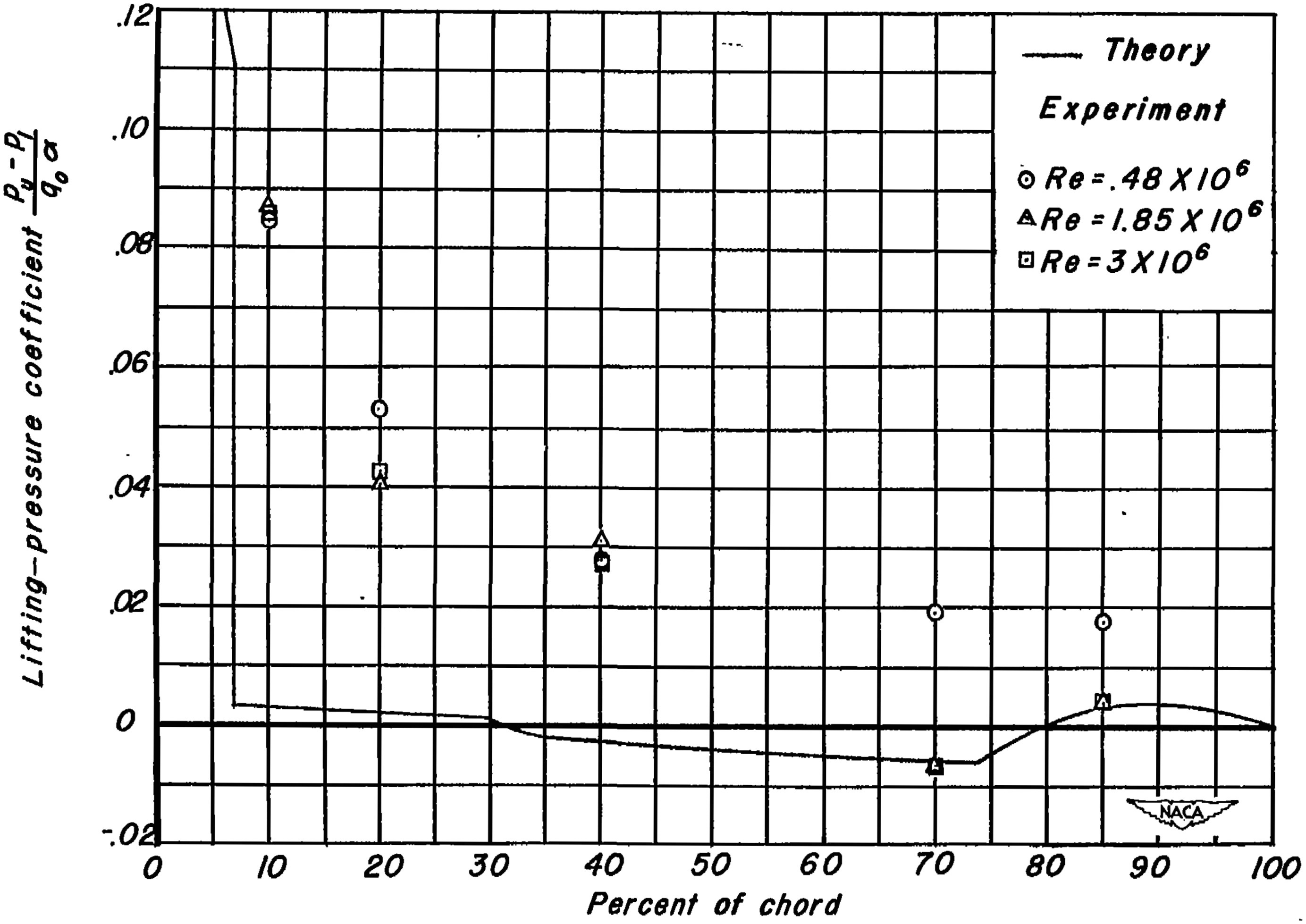

(e) 97.5 % Semispan.

Figure 6.—Concluded.

[redacted]

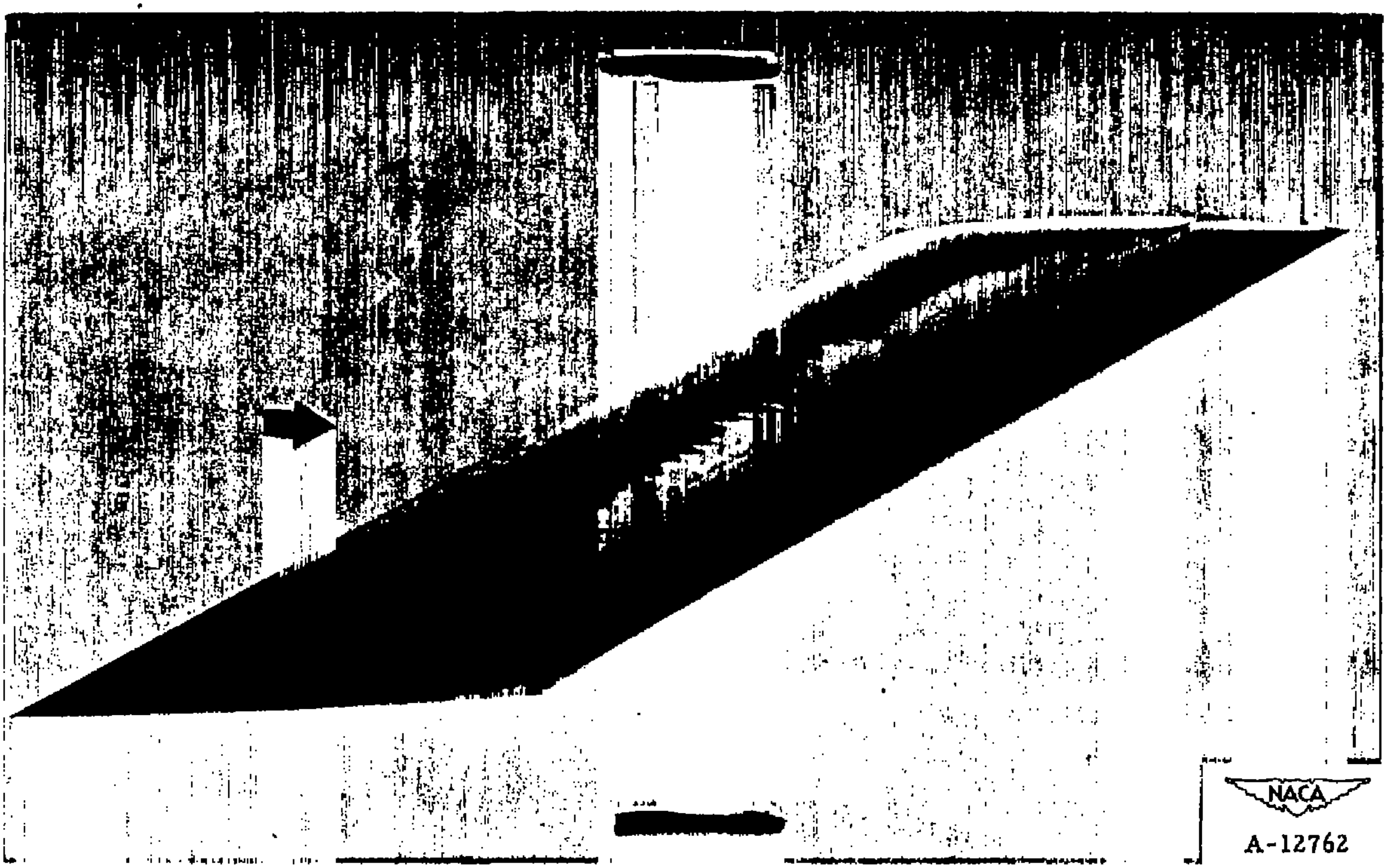

NACA
A-12762

(a) $\alpha = 0^\circ$.

Figure 7.— Photographs of liquid film at $M = 1.53$. $Re = 3.0 \times 10^6$.

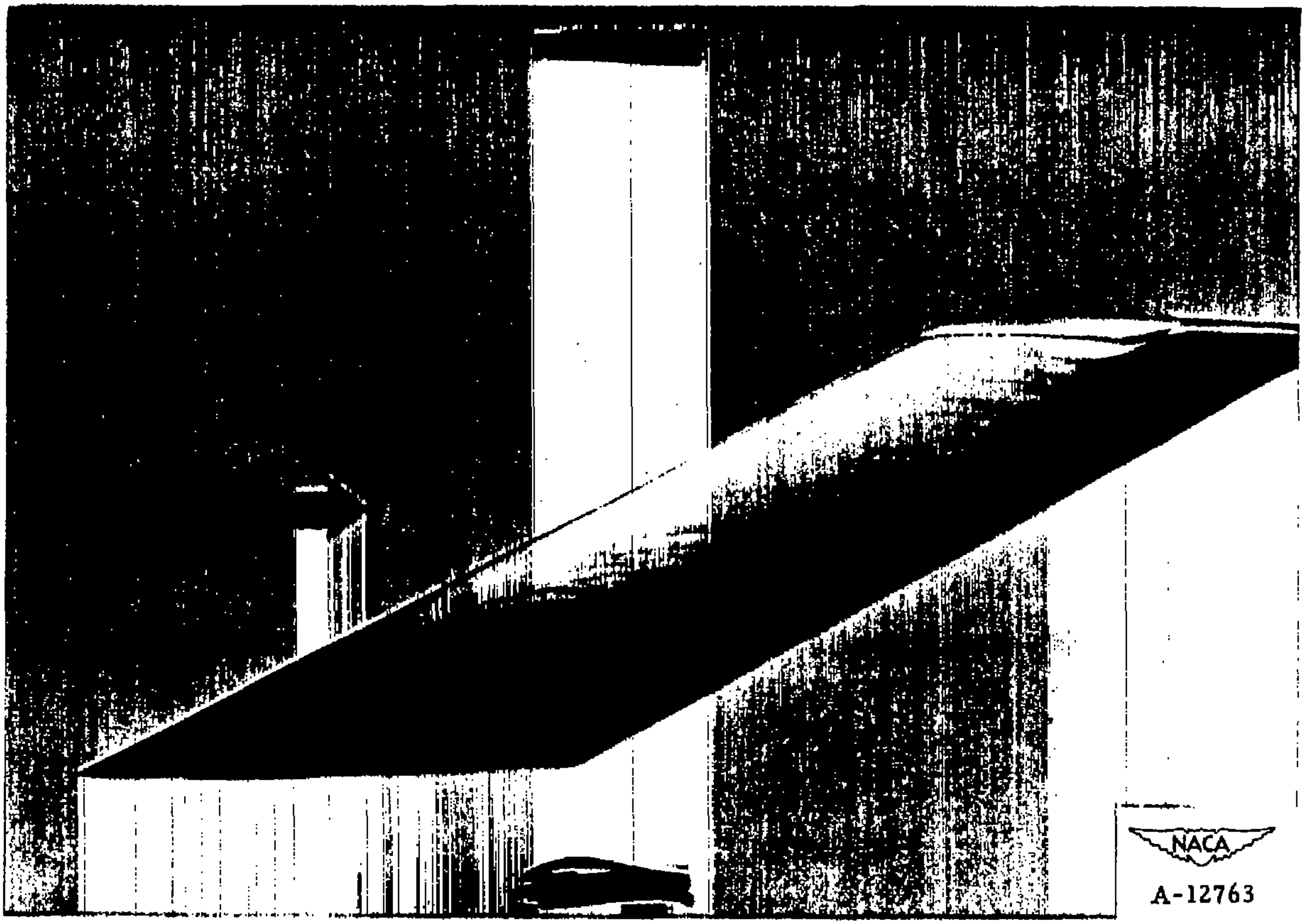
NACA
A-12763

(b) $\alpha = 4^{\circ}$.

Figure 7.– Continued.

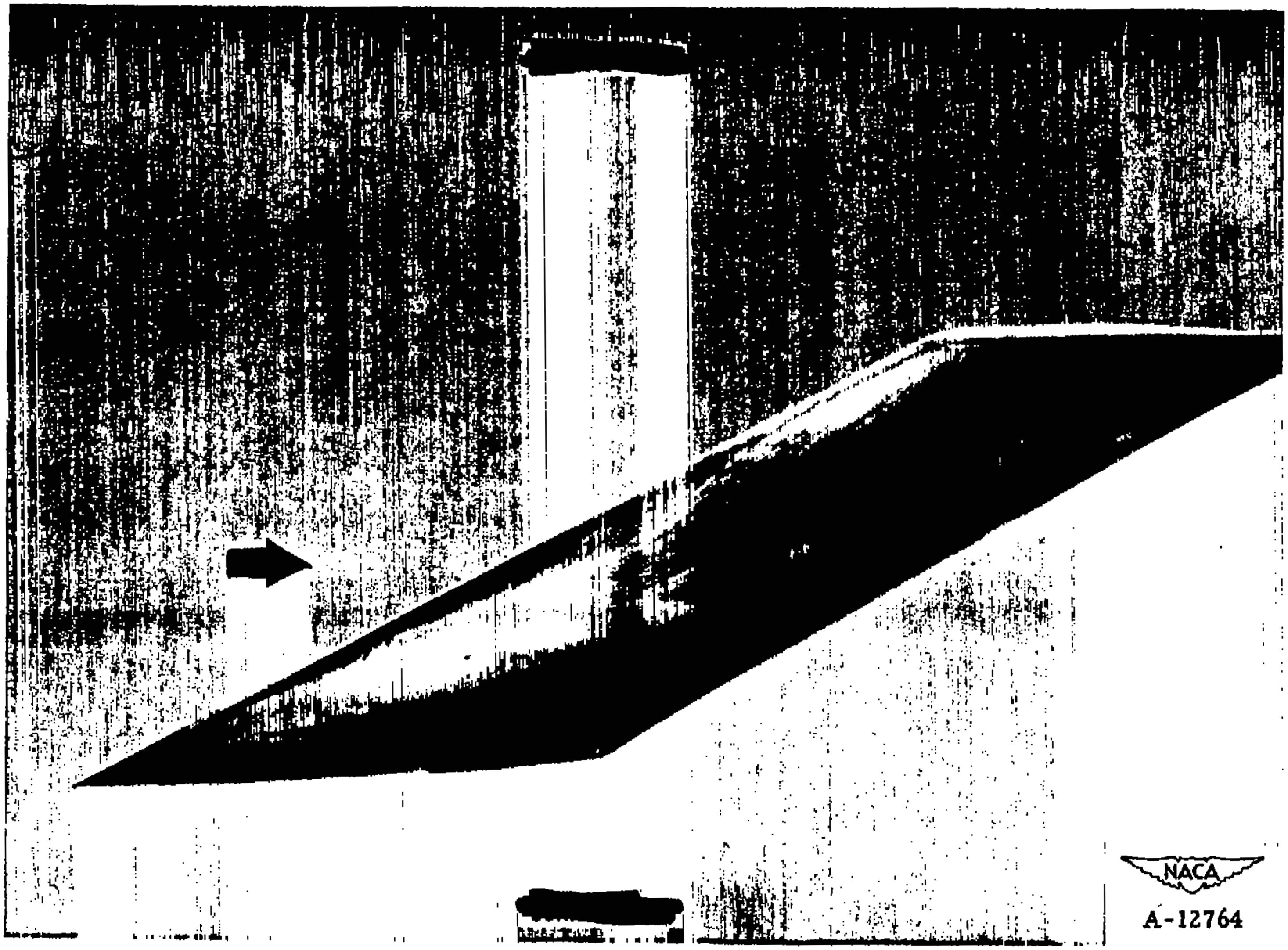
NACA
A-12764

(c) $\alpha = 8^{\circ}$.

Figure 7.– Concluded.

[redacted]

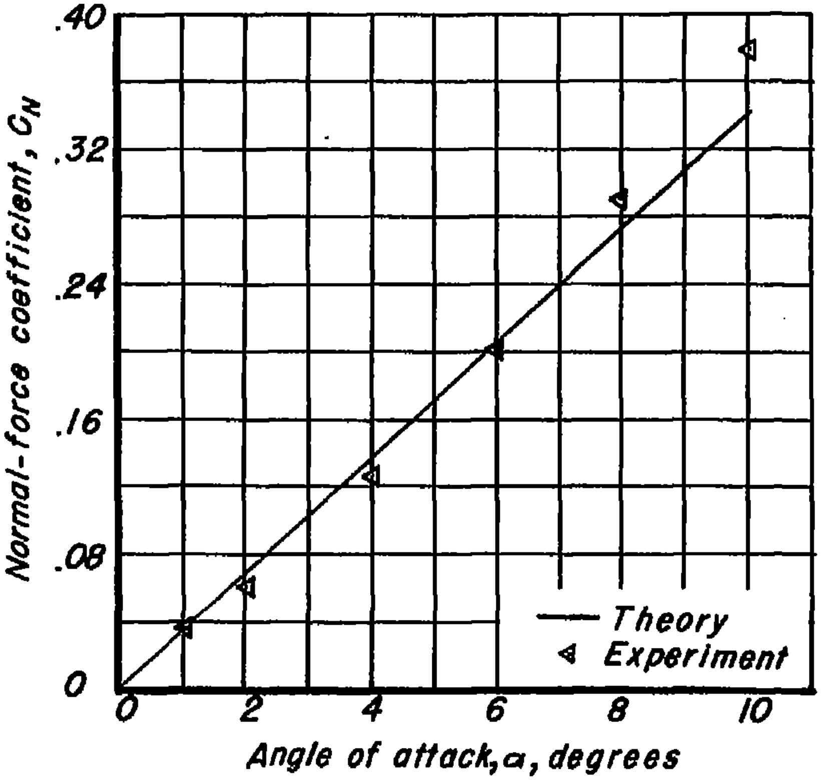

Figure 8.—Variation of normal-force coefficient with angle of attack. $Re = 3 \times 10^6$

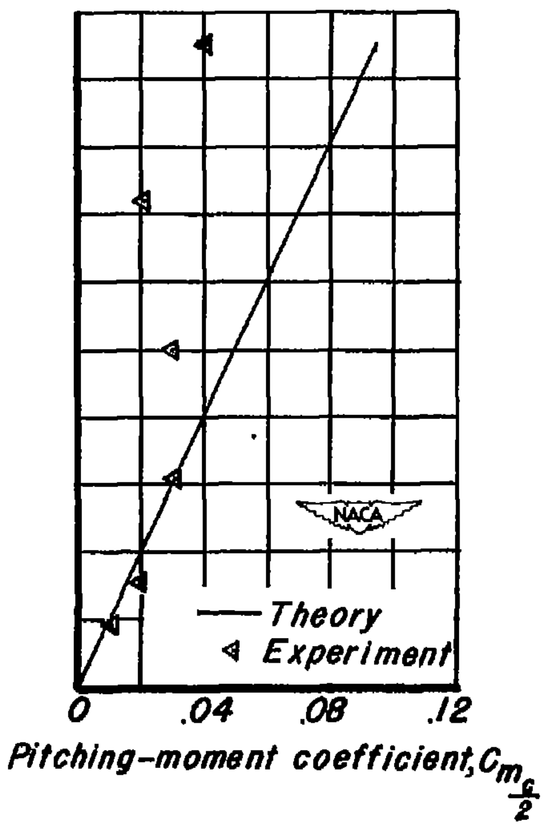

Figure 9.—Variation of pitching-moment coefficient about centroid of area with normal-force coefficient. $Re = 3 \times 10^6$

[redacted]

NASA Technical Library
3 1176 01434 4601